Petroleum Science 20 (2023) 1327–1346

Contents lists available at ScienceDirect

Petroleum Science

journal homepage: www.keaipublishing.com/en/journals/petroleum-science

Original Paper

Organic matter accumulation in lacustrine shale of the Permian Jimsar Sag, Junggar Basin, NW China

Xiu-Jian Ding [a, *], Wen-Jun He [b], Hai-Lei Liu [b], Xu-Guang Guo [b], Ming Zha [a], Zhong-Fa Jiang [b]

[a] School of Geosciences in China University of Petroleum, Qingdao, Shandong, 266580, China
[b] Research Institute of Petroleum Exploration and Development, PetroChina Xinjiang Oilfield Company, Karamay, Xinjiang, 841000, China

ARTICLE INFO

Article history:
Received 18 November 2021
Received in revised form
29 August 2022
Accepted 1 November 2022
Available online 9 November 2022

Edited by Jia-Jia Fei and Teng Zhu

Keywords:
Lucaogou formation
Jimsar sag
Organic-matter-rich shale
Organic matter accumulation
Organic matter productivity
Bacterial sulfate reduction

ABSTRACT

The lacustrine organic-rich shale in the Permian Lucaogou (LCG) Formation of the Jimsar Sag, Junggar Basin, is one of the main shale oil plays in China. In this paper, geological and geochemical research techniques were employed to evaluate the geochemical variability of the lacustrine shale and the production of organic matter and its preservation conditions. The LCG Formation is characterized by its complex mineral compositions and a wide range of organic matter richness and quality. The presence of high proportions of β-carotane and C_{29} steranes, indicates that the organic matter mainly originated from phytoplankton and aquatic algal-bacterial organisms, especially cyanobacteria. This study found that the productivity of the Lower LCG Member (P_2l_1) was highest, and the Middle LCG Member (P_2l_2) was the lowest. During the deposition of the Lower LCG Member, the lake's bottom water was predominantly a reducing environment, and the degradation of organic matter was largely a result of bacterial sulfate reduction. During the deposition of the Middle and Upper LCG members, the lake's bottom water was mainly oxidizing, and the degradation of organic matter was likely to be caused by aerobic processes. Based on a comprehensive analysis of the origin and production of organic matter, as well as its depositional environment and preservation conditions, two organic matter accumulation models were proposed to explain the distribution of the organic-rich shale. In model A, the high influx of volcanic ash released nutrients and brought abundant sulfate into the water, the accumulation of organic matter was mainly controlled by the preservation of organic matter, which was mainly controlled by BSR. In the model B, the influx of volcanic ash was small, organic matter was mainly degraded by oxygen and the accumulation of organic matter is mainly determined by the production of organic matter.

1. Introduction

Organic-matter-rich shales are the main target rocks for unconventional oil and gas exploration and development around the world (Jarvie et al., 2007; Katz and Lin, 2014; Zou et al., 2019). Lacustrine shales show growing potential for conventional and unconventional petroleum exploration, especially in China (Carroll and Bohacs, 2001; Zou et al., 2015; Hu et al., 2021). Previous studies show that lacustrine organic-matter-rich sediments may feature strong variations in geochemical characteristics and hydrocarbon (HC) potential (Keym et al., 2006; Hao et al., 2011; Katz and Lin, 2014; Li et al., 2017). Lacustrine organic-rich sediments have the potential for significant petroleum resources (Hao et al., 2011; Hu et al., 2022), especially unconventional resources, such as tight oil and gas, and shale oil and gas (Zou et al., 2019; Cao et al., 2021).

Based on different tectonic settings and depositional processes of modern and ancient lakes, many models have been proposed for the development of lacustrine organic-rich sediments (Hao et al., 2011), such as the stratified lake and the playa-lake model of the Green River Formation (Bradley, 1970; Eugster and Surdam, 1973), the deep anoxic lake model (Demaison and Moore, 1980), the large mesosaline alkaline closed lake model (Kelts, 1988), the moderately deep tropical lake model (Katz, 1990), and the small shallow lake model (Ding et al., 2015, 2016).

The Permian Lucaogou Formation (LCG) within the Jimsar Sag is characterized by a complex mineral composition (Xi et al., 2015; Zheng et al., 2016; Wang et al., 2020; Yang et al., 2022) and abudant

* Corresponding author. School of Geosciences in China University of Petroleum, Qingdao, Shandong, 266580, China
E-mail addresses: dingxj@upc.edu.cn, dingxj129@foxmail.com (X.-J. Ding).

https://doi.org/10.1016/j.petsci.2022.11.004

organic matter (Liu et al., 2012; Liu et al., 2022). Terrigenous detrital material, carbonates and volcanic ash also are components of LCG. The volcanic material may have influenced lake water chemistry and depositional environment, thus playing a role in the productivity and preservation of organic matter (Langmann et al., 2010; Turgeon and Creaser, 2008; Morel and Price, 2003). Previous studies on LCG organic-rich shales were mainly dealing with its geochemical or source rock character addressing organic matter richness, type, and maturity (Cao et al., 2015, 2016; Qiu et al., 2016a; Hu et al., 2017; Ding et al., 2017). There has been little discussion on the production, preservation, and accumulation of organic matter, including the role of volcanic ash in these processes.

This study represents a comprehensive examination of the Permian LCG organic-rich shale, which includes the geochemical and petrological features of the lacustrine source rock, the origin, production and preservation of organic matter, and the evolution of the depositional environment. Accumulation models are then proposed for lacustrine organic-rich shales based on integrating geological and geochemical data. These models should provide insight into study of organic-rich shale and shale oil exploration in other lacustrine basins.

2. Geologic setting

The Jimsar Sag, with an area of 1278 km^2, is located in the eastern uplift of the Junggar Basin (Fig. 1). It is one of the main petroliferous basins in northwestern China (Chen et al., 2016; Tang et al., 2021; Hou et al., 2021). Recent advancements in shale oil exploration have led to the discovery of an estimated 17.85 billion barrels of geologic hydrocarbon resources (Qiu et al., 2016b). With the discovery of a large amount of tight oil and shale oil, the Jimsar Sag has become a hot spot for unconventional resource exploration in China (Wang et al., 2015; Jiang et al., 2015; Jin et al., 2021).

The Jimsar Sag is a dustpan-shaped depression and has a gentle structure, with a boundary fault in the west and stratigraphic overlap in the east (Fig. 2). The basement is an Upper Carboniferous flexure, with a Permian to Quaternary sedimentary cover. The sag has undergone multistage tectonic movements, including the Hercynian, Indosinian, Yanshan and Himalayan, since the Carboniferous Period (Yang et al., 2017). As a result, the LCG Formation is thick in the west and south rims and pinchs out gradually towards the east rim (Figs. 1b and 2).

The Permian LCG Formation contains abundant organic matter (mainly kerogen type II), making it a high-quality source rock with high hydrocarbon generation potential (Kuang et al., 2012, 2022). The organic-rich shale, with a thickness of 200–300 m, is the target formation of shale oil exploration in the sag (Luo et al., 2018) (Fig. 1c). The LCG Formation was mainly deposited in a saline lacustrine environment, with a large influx of authigenic sediments, volcanic materials, and terrigenous clastic materials. The LCG Formation is characterized by thin monolayers and frequently alternating lithologies (Shao et al., 2015; Pang et al., 2022) and can be further divided into Lower (P_2l_1), Middle (P_2l_2) and Upper (P_2l_3) members.

3. Samples and methods

Samples from the LCG Formation were collected from cores of an exploration well in the Jimsar Sag, as shown in Fig. 1b. More than 200 samples were obtained for such analyses as X-ray diffraction, total organic carbon (TOC) measurements, Rock-Eval pyrolysis and gas chromatography-mass spectrometry (GC-MS).

Seventy core samples were analyzed for whole-rock (bulk) mineralogy using a DRON 3M Powder X-ray diffractometer. Preparation, analysis, and interpretation of the samples follow the procedure outlined by Hillier (2003), and results are shown in Appendix Table 1.

TOC values were measured using a LECO-CS-230 carbon/sulfur analyzer. Before the analysis, all powdered samples were treated with HCl at 60 °C for 24 h to remove carbonates and then washed with distilled water to remove the HCl. Pyrolysis was then carried out to measure T_{max}, S_1, and S_2 using a Rock-Eval VI instrument, according to the China National Standard of rock pyrolysis analysis GB/T18602-2012, as described by Cao et al. (2018). Where S_1 is the amount of free hydrocarbons volatilized from the rock sample (mg of HC/g of rock), S_2 is the amount of hydrocarbons produced as a result of the cracking of organic matter (mg of HC/g of rock), and T_{max} (°C) is the temperature at which the amount of hydrocarbon generation from kerogen cracking reaches its maximum. In the experiment, the powdered sample was heated to 300 °C in a helium atmosphere such that S_1 was measured. Then the sample is heated continuously from 300 °C to 600 °C at a constant rate of 25 °C/min, during which S_2 and T_{max} were measured. The TOC and Rock-Eval results are summarized in Appendix Table 2.

A total of 62 core samples were powdered, extracted and separated into saturate, aromatic and polar fractions for gas chromatography-mass spectrometry (GC-MS) analysis. Soxhlet extraction was conducted using a chloroform/methanol solution (87:13, *v*/*v*) for 72 h. The extractable organic matter was separated into saturated hydrocarbon, aromatic hydrocarbon and polar fractions. The saturated hydrocarbon fraction was dissolved in hexane and analyzed by gas chromatography (GC) using an HP-5MS column, with the temperature programmed to increase from 40 °C to 300 °C at a rate of 4 °C/min, and then held at 300 °C for 30 min. The GC-MS analyses of the saturated fraction were performed using an HP6890GC/5973MSD instrument, equipped with an HP-5MS fused silica column (30 m × 0.25 mm, i. d., film thickness 0.25 μm). The GC oven temperature for analysis of the saturate fractions was held at 50 °C for 2 min, then programmed to increase to 100 °C at 20 °C/min, then to 310 °C at 3 °C/min, before being held at 310 °C for 16.5 min. Biomarker ratios were calculated from the peak areas of individual compounds, with results summarized in Appendix Table 3.

4. Results

4.1. Mineralogy and petrography

Thin-section examination and XRD study show that LCG organic-rich shales are characterized by a complex mineral composition with various rock components, including quartz, plagioclase, K-feldspar, clay, dolomite, ankerite, calcite, and pyrite (Fig. 3; Appendix Table 1).

Quartz is one of the main mineral constituents, accounting for 8.2 wt% to 39.3 wt%, with an average of 20.8 wt% with no obvious trend across the entire LCG. The average plagioclase content is 23.3 wt%, similar to that of quartz, but with a broader range from 3.0 wt% to 49.8 wt%. Plagioclase content increases from the Lower LCG Member to the Upper LCG Member. K-feldspar is less abundant than plagioclase, ranging from 0.6 wt% to 13.1 wt% and low in the Middle LCG Member. Clay content ranges from 0.9 wt% to 35.9 wt% (10.8 wt% average) and is relatively higher in the Middle LCG Member. The dolomite content has the largest range from 7.5 wt% to 80.1 wt% (27.7 wt% average). A weak increasing trend in dolomite content is observed from the Lower to Upper LCG Member. The content of other minerals, such as ankerite, calcite, pyrite, and zeolite minerals, are very low. It is worthy of note that the content of calcite and pyrite from the Lower LCG Member are much higher than that from the Middle and Upper LCG members.

Dolomites, mudstones, tuffites and siltstones are four

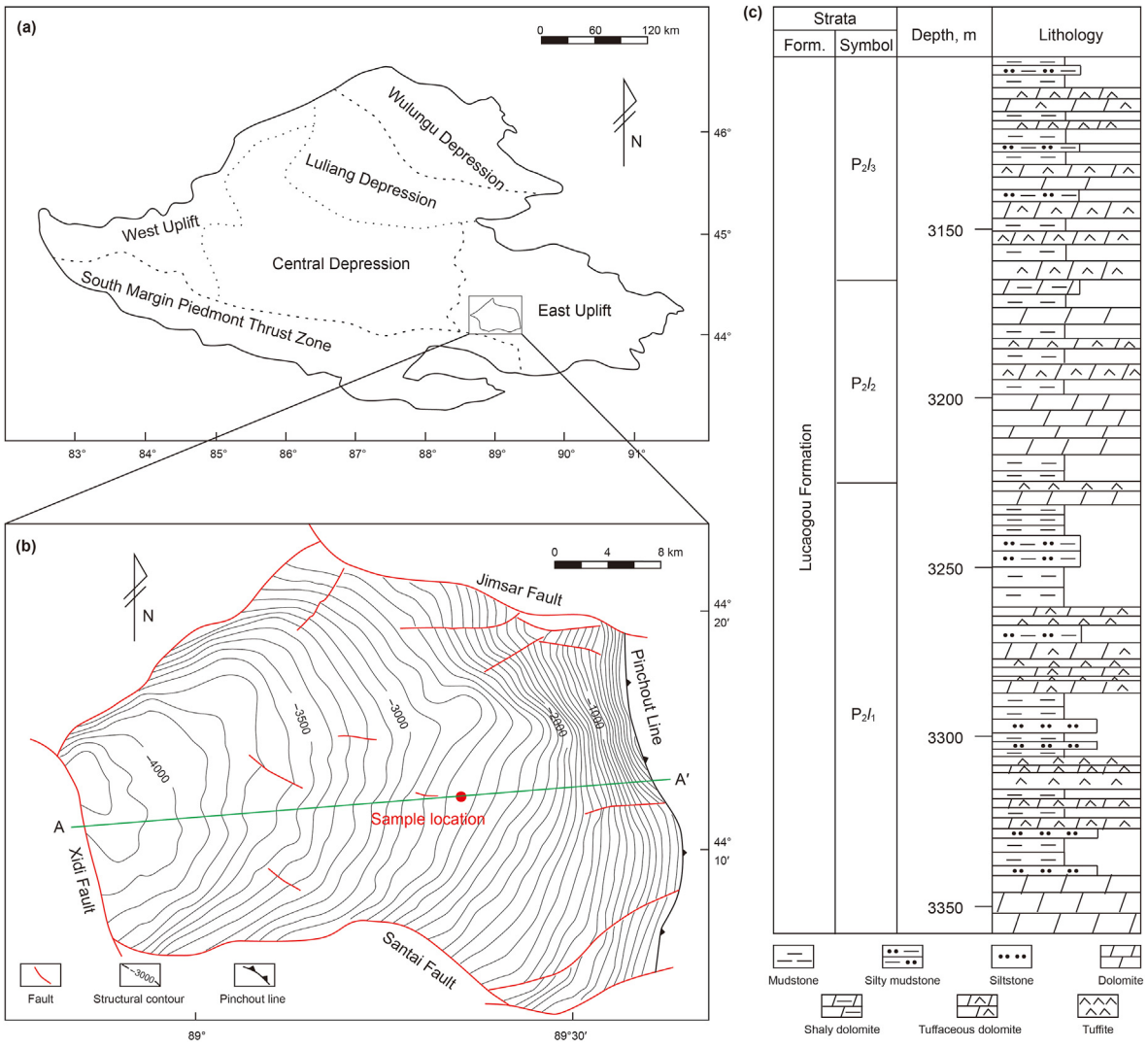

Fig. 1. (**a**) Map of the Junggar Basin in northwestern China, showing the location of the Jimsar Sag; (**b**) structure contour map of the surface of the Lucaogou Formation in the Jimsar Sag, showing the well from which core samples were taken; (**c**) a summary of the lithostratigraphy of the Jimsar Sag (modified after Jiang et al., 2015). Form. = Formation.

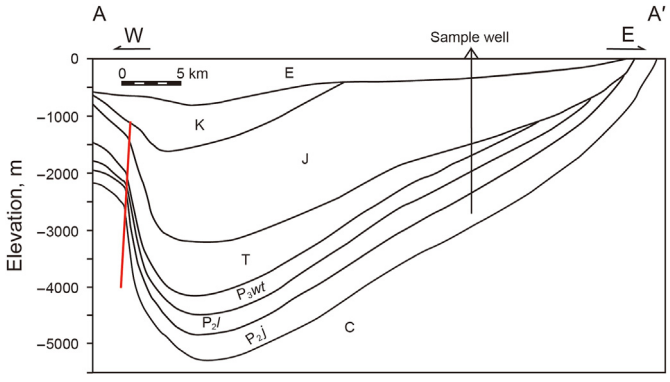

Fig. 2. Geological cross-section of the Jimsar Sag for the segment AA′ in Fig. 1.

predominant rock types identified based on cores and thin section observations, shown in Fig. 4. Complex grain assemblages with various mixtures of extrabasinal detrital components, intrabasinal carbonate components, and volcaniclastic components were observed. For instance, dolomites comprise of a large proportion of intraclast and micrite components with a small proportion of siliciclastic grains and tuffaceous components. Feldspar and detritus are the predominant components in the siltstones with a low proportion of carbonate or tuffaceous material. Framboidal pyrite and vitroclastics are very common and can be easily identified using the scanning electron microscope (Fig. 4). In summary, the mineralogy and petrography indicate that the LCG Formation is composed of a regularly alternating sequence of mudstone, dolomitic sandstone, detrital dolomite, dolomite and tuffite.

4.2. TOC and Rock-Eval

The LCG Formation exhibits a wide range of TOC contents, from 0.34% to 10.58% with mean value of 3.20% (Table 2, Fig. 5). In general, there are no significant trends in TOC contents across the entire LCG Formation. However, it should be noted that the heterogeneity of TOC content is greater in the Lower and Upper LCG members than the Middle LCG Member, where both the highest and lowest TOC content values were seen. It seems that there may be weak trend of decreasing first and then increasing TOC content

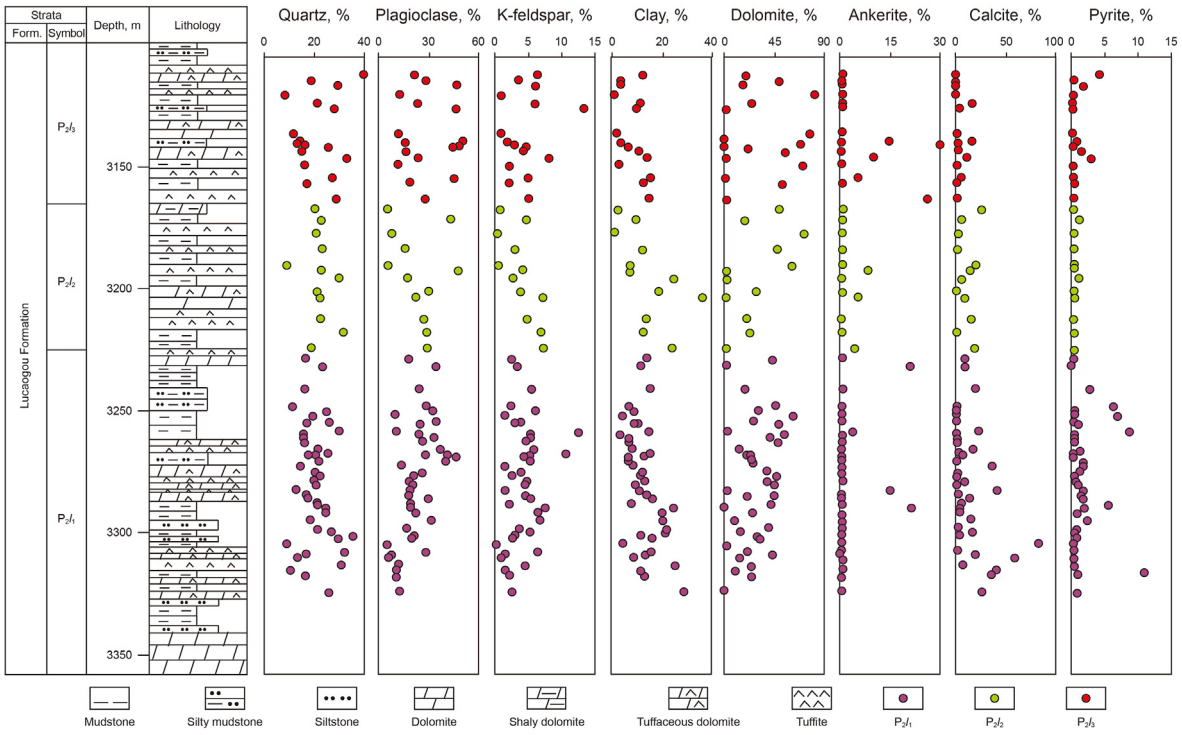

Fig. 3. Variations of mineral contents reflecting mineral composition of the Lower Permian Lucaogou shale in the Jimsar Sag as a function of burial depth.

from the bottom to the top of LCG Formation.

The values of S_2 show a similar distribution as TOC content, with relatively high values in the Lower and Upper LCG members. The hydrocarbon generation index (S_1+S_2) is in the range of 0.32–66.54 mg/g, with a mean value of 12.69 mg/g (Table 2, Fig. 5). Generally, anything above 6.0 mg HC/g is indicative of high hydrocarbon potential (Peters et al., 1999). The HI (S_2/TOC) value initialy decreases, then increases, and at last decreases again from the bottom to the top of LCG Formation, with the relatively high values mainly distributed in the Lower and Upper LCG members.

4.3. Organic matter microscopic component

Polished blocks were examined for the identification and description of maceral groups containing liptinite, vitrinite, inertinite, and bitumen. According to the well-established ICCP liptinite classification (Sýkorová et al., 2005), the liptinite group includes bituminite, alginite, cutinite, sporinite, suberinite, resinite, exsudatinite and liptodetrinite. In the LCG organic-matter-rich shales, bituminite and alginite are found to be relatively abundant; whereas, cutinite, sporinite and liptodetrinite are less abundant. The bituminite features three distribution patterns: 1) locally agglomerated and surrounded by minerals (Fig. 6a), 2) stripe-like and parallel with formation bedding (Fig. 6b) and 3) finely dispersed within the mineral-bituminous groundmass (Fig. 6c). Compared with bituminite, alginite has a more pronounced yellow fluorescence (Fig. 6d and e). The alginite is found to be well-preserved and observed in several samples.

Vitrinite, with a particle size of 10–100 μm, were mainly transported and deposited along with mineral matter (Fig. 6g and f). Under incident blue light, inertinite shows no fluorescence; under reflected white light, its reflection is stronger than vitrinite but weaker than pyrite (Fig. 6h). Bitumen occurs mainly in pores and micro-fractures as a byproduct of the hydrocarbon generation or migration process (Fig. 6i).

4.4. Molecular biomarkers analysis

Biomarkers have drawn much attention over the past few decades, mainly because of their utility in assessing organic matter origin and depositional conditions (e.g. salinity, redox conditions, etc.) (Peters et al., 2005). The distribution of biomarkers in the LCG organic-matter-rich shale samples is shown in Fig. 7.

The organic-matter-rich sediment extracts contain a full range of C_{13}–C_{31} *n*-alkanes and isoprenoids, including pristane and phytane. The *n*-alkane patterns including both short chain (nC_{12}–nC_{21}) and long chain (nC_{22}–nC_{35}) *n*-alkanes (Fig. 7). The samples display pristane/phytane (Pr/Ph) between 0.74 and 2.10, Pr/*n*-C_{17} between 0.15 and 2.25 and Ph/*n*-C_{18} between 0.09 and 3.08 (Fig. 7 and Appendix Table 3). The analyzed samples display wide variations in the relative abundance of pristane, *n*-C_{17}, phytane, *n*-C_{18} and β-carotane, suggesting changes in depositional environment and original biomass.

The gammacerane/C_{30}hopane of the samples ranges from 0.07 to 0.27, with average of 0.17 (Fig. 7 and Appendix Table 3). The analyzed samples has C_{27}sterane 20R/(C_{27}sterane 20R + C_{28}sterane 20R + C_{29}sterane 20R) ranging from 6.32 to 28.54, C_{28}sterane 20R/(C_{27}sterane 20R + C_{28}sterane 20R + C_{29}sterane 20R) ranging from 28.72 to 57.26, C_{29}sterane 20R/(C_{27}sterane 20R + C_{28}sterane 20R + C_{29}sterane 20R) ranging from 28.05 to 60.93 (Fig. 7 and Appendix Table 3). The wide variation in the relative abundance shown by terpane and sterane series, such as tricyclic terpanes, Ts, Tm, gammacerane, C_{27} steranes, C_{28} steranes and C_{29} steranes, is interpreted here to reflect differences in organic matter input and water salinity.

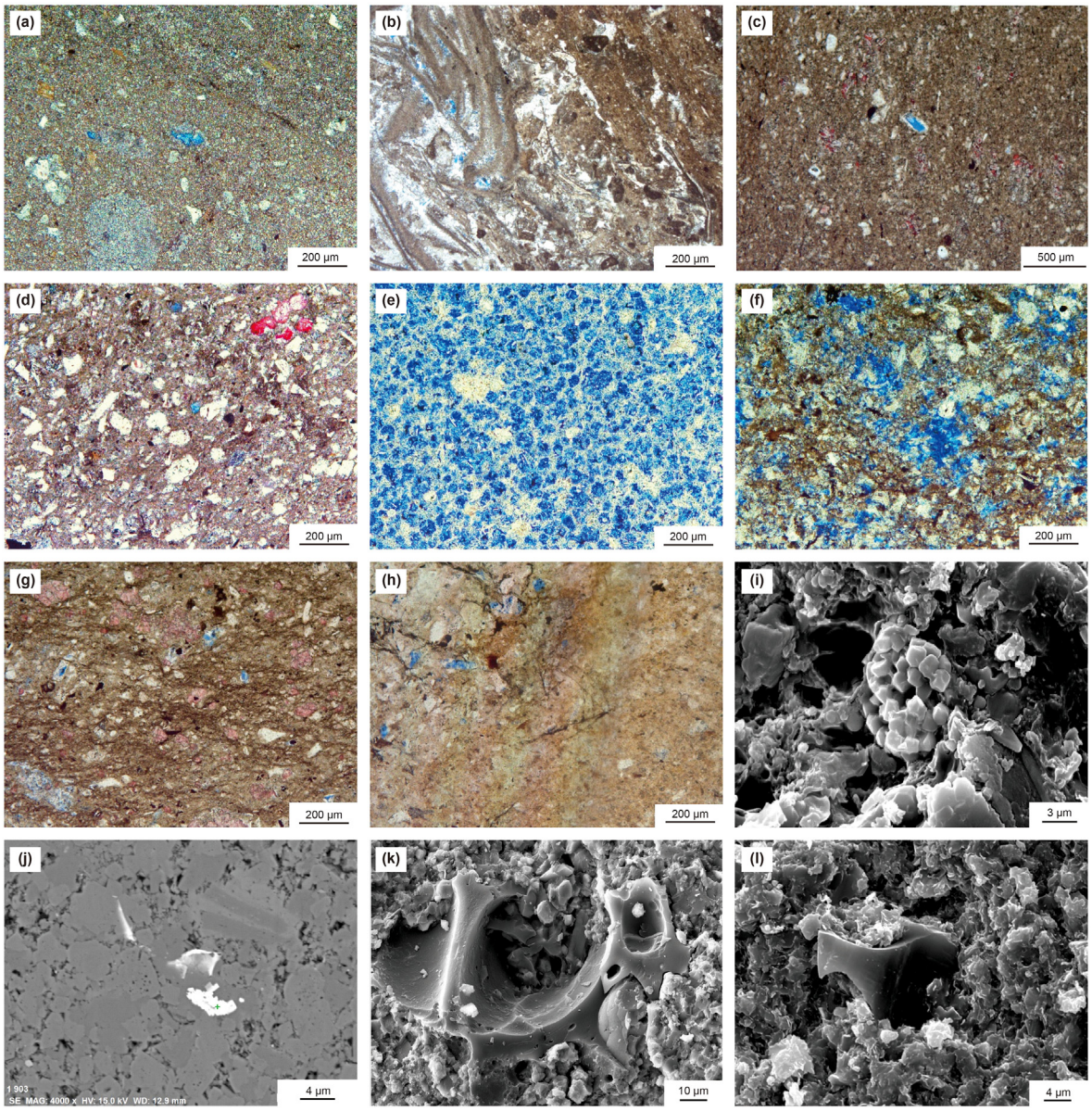

Fig. 4. Photomicrographs of thin sections of single polarized light (blue epoxy resin-impregnated) and scanning electron microscope (SEM) images of the Lower Permian Lucaogou Formation in the Jimsar Sag showing lithology and mineral: (**a**) 3138.76 m, dolomite; (**b**) 3151.31 m, bioclastic dolomitic mudstone; (**c**) 3210.69 m, silty dolomitic mudstone; (**d**), 3241.89 m, tuffaceous silty mudstone; (**e**) 3262.59 m, tuffite; (**f**) 3283.74 m, dolomitic siltstone; (**g**) 3306.97 m, limy silty mudstone; (**h**) 3328.48 m, dolomitic mudstone; (**I**) 3152.98 m, framboidal pyrite; (**J**) 3284.20 m, framboidal pyrite; (**k**) 3125.08 m, vitroclastic; (**I**) 3332.81 m, vitroclastic.

5. Discussion

5.1. Quality of source rocks

A Rock-Eval S_2 vs. TOC content in log scale is shown in Fig. 8 for three groups (Upper-Middle-Lower) of LCG Formation. The quality of source rock can be evaluated as poor source rock, fair source rock, and good to excellent source rock (Peters and Cassa, 1991). Most of the samples are plot in the fair to excellent source rock areas with TOC contents greater than 1.0%, and S_2 values greater than 2 mg HC/g. There are some subtle variations in the vertical trends from the Lower to Upper LCG members. Generally speaking, the average source rock quality of the Middle LCG Member is better than that of Lower and Upper LCG for two reasons: 1) it is more homogeneous; and 2) the presence of poor-quality source rock is nominal.

The wide HI range as demonstrated in Fig. 9, shows that kerogen compositions of the organic-rich shale in the Lucaogou Formation vary significantly, indicating different origins of the organic matter or preservation state. The majority of the samples belong to Type II or Type III kerogen (Fig. 9) (Peters, 1986; Huang et al., 1984).

In the HI vs. TOC plot (Fig. 10), there is a generalized positive correlation between TOC and HI, therefore indicating that the organic matter in the shale samples is mainly from algae and plankton.

In addition, T_{max} values of the samples range from 441 °C to 455 °C, implying the thermal evolution of the organic matter is between the immature and mature stage (Table 2, Fig. 9). This is also supported by the R_o (vitrinite reflectance, range of 0.53%–1.31%) in Kou's study (Kou, 2015).

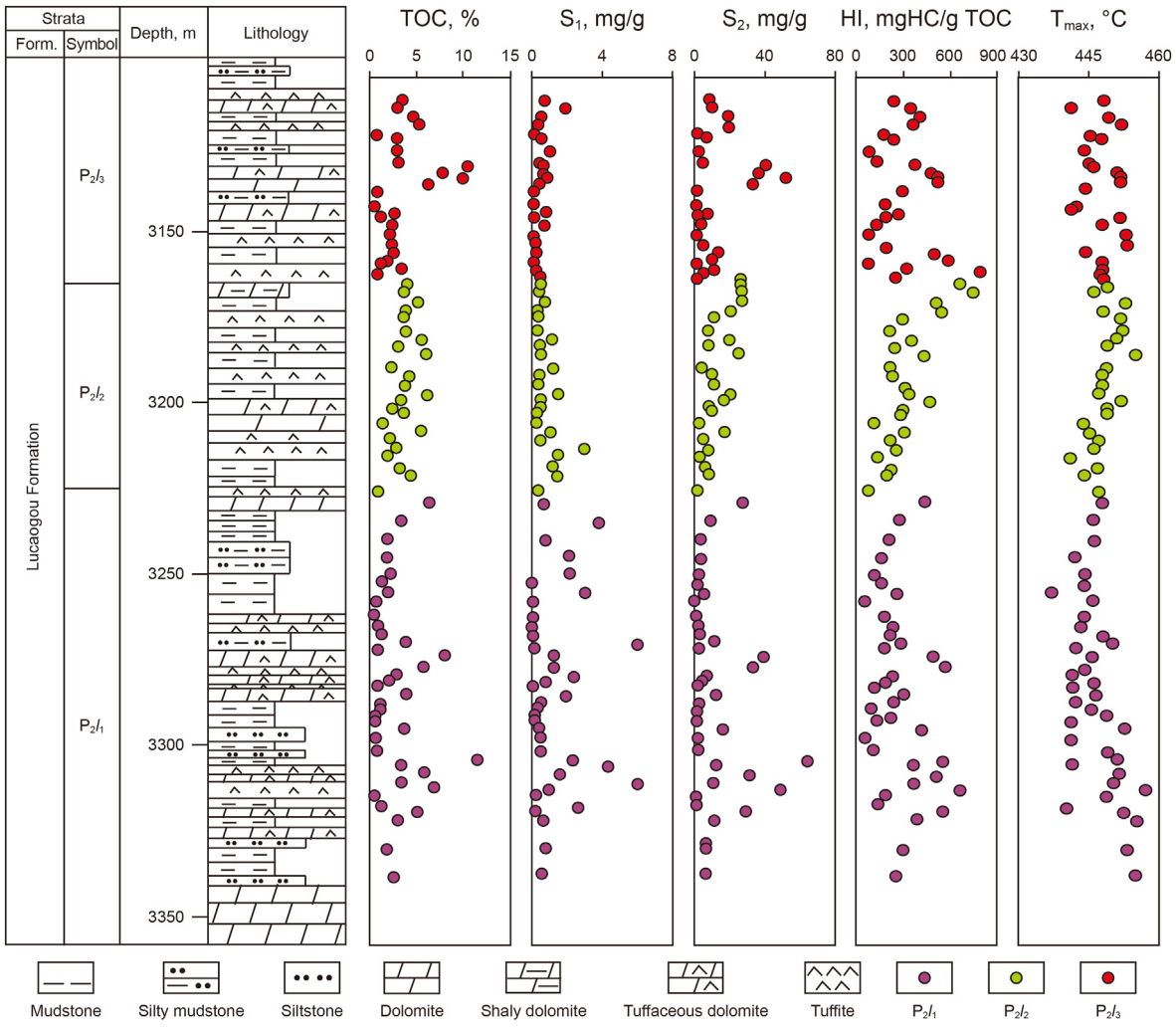

Fig. 5. Vertical variations in TOC, S_1, HI and T_{max} data for shale within the Lower Permian Lucaogou Formation in the Jimsar Sag of the Junggar Basin. Abbreviations are explained in Table 2.

5.2. Origin and production of organic matter

The distribution patterns of *n*-alkanes provide information about the origin of organic matter. For example, long chain *n*-alkanes (C_{22}–C_{35}) are mainly derived from higher terrestrial plants and short chain *n*-alkanes (C_{12}–C_{21}) are typically derived from algae and plankton (Eglinton and Hamilton, 1967; Cranwell et al., 1987; Meyers, 1997). The nC_{21-}/nC_{22+} ratios of the LCG Formation are in the range of 0.5–2.0, with most organic matter being short chain *n*-alkanes (C_{12}–C_{21}) (Fig. 11 and Appendix Table 3), indicating that the majority of LCG Formation organic matter was likely to be derived from an algal or planktonic source. It also suggests that the algal and planktonic sources of organic matter are more common in the Lower LCG Member than in the Middle and Upper LCG members.

Proportional sterane abundances are very useful indicators for qualitative shifts in biological sources of organic matter (Seifert and Moldowan, 1978). As shown in Appendix Table 3 and Fig. 11, the most abundant steranes of the LCG organic-matter-rich shale samples are C_{29} (28%–61%, average 47%), followed by C_{28} (29%–57%, average 37%), with minimal C_{27} steranes (6%–29%, average 16%). Usually, C_{29} and C_{27} steranes are mainly derived from terrigenous higher plants and phytoplankton, respectively, whereas C_{28} steranes normally originate from special phytoplankton, such as diatoms (Hao et al., 2011).

Low intrinsic C_{27} steranes and high intrinsic C_{29} steranes of the LCG organic matter are generally believed to be mainly derived from higher terrestrial plants rather than the phytoplankton or aquatic algal-bacterial organisms. However, due to the relatively high abundance of bituminite and alginite in the samples, coupled with cyanobacteria being an important source of C_{29} steranes (Volkman, 1983; Volkman et al., 1998). It is believed that the cyanobacteria is the primary source of the organic matter in the LCG Formation, with higher terrestrial plants being secondary.

Another observation is the relatively high β-carotane/C_{max} values (up to 2.82 in Appendix Table 3). The β-carotane is associated primarily with anoxic or highly restricted marine settings, as well as saline lacustrine environments (Hall and Douglas, 1983). Ding et al. (2017) and Ding W.J. et al. (2019) indicated that the β-carotane content of LCG Formation in the Jimsar Sag is controlled by the source of organic matter rather than the redox condition, and that there is a positive correlation between β/C_{max} values and C_{29} steranes proportion of the LCG Formation. Philp et al. (1992) and Peters et al. (2005) showed that the main biological source of β-carotane are cyanobacteria. In addition, Philp et al. (1992) demonstrated that β-carotane content did not show any direct

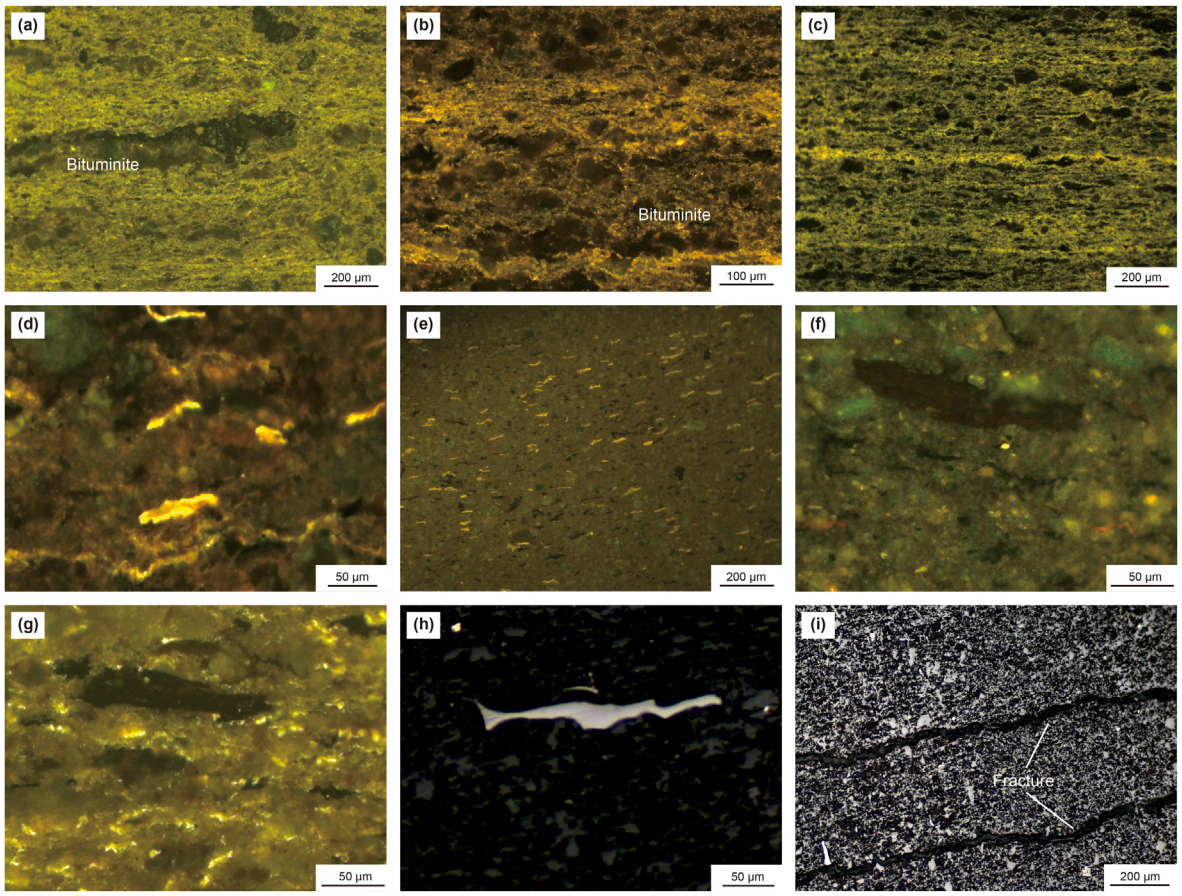

Fig. 6. Photomicrographs of organic matter in the polished blocks: (**a**)–(**c**), bituminite under incident blue light; (**d**)–(**e**), alginite under incident blue light; (**f**)–(**g**), vitrinite under incident blue light; (**h**), inertinite under reflected white light; (**i**), bitumen in fractures.

relationship with salinity, redox conditions, or depositional environment in the Biyang Basin of China. It is, therefore, concluded that both β-carotane and C_{29} steranes were mainly originated from cyanobacteria and that β-carotane can be used as an indicator of the source of organic matter.

The above biomarker analysis shows that the organic matter in the LCG Formation was likely originated from phytoplankton and aquatic algal-bacterial organisms, especially cyanobacteria. Therefore, the content of aquatic organisms in the Lower LCG Member is the highest, followed by the Upper LCG Member, and the lowest in the Middle LCG Member. This is supported by the relative sterane content, β-carotane content and C_{21-}/C_{22+} ratio.

Carbon isotopic composition of lacustrine carbonate sediments is a key indicator of organic matter productivity of ancient lakes (Mckenzie, 1982; Sarnthein and Winn, 1990; Isozaki et al., 2007). The greater the productivity, the more ^{12}C is incorporated into the biomass. At the same time, carbonates formed in the water, have an enriched ^{13}C content, thus an increased level of $\delta^{13}C$. Therefore, carbon isotopic composition in carbonates precipitated *in situ* is a valid proxy for organic matter productivity in lacustrine sediments (Oana and Deevey, 1960; Mckenzie, 1982, 1985).

The $\delta^{13}C_{carb}$ value is also widely used in the studies of the global carbon cycle (Marcel and Vernal, 2007), chemical evolution of seawater (Kaufman and Knoll, 1995), and even salinity (Fischer and Wefer, 1999). Because carbon isotopic composition is less affected by diagenesis (Anderson and Arthur, 1983; Magaritz, 1983; Glumac and Spivak-Birndorf, 2002), the drastic changes in $\delta^{13}C_{carb}$ over geological time are attributed to significant changes in organic matter productivity of water (Hoffman et al., 1998; Hoefs, 2009). The $\delta^{13}C_{carb}$ value of the samples from the LCG Formation varies significantly between 2.73‰ and 11.7‰, with an average of 7.8‰ (Wu et al., 2017), corresponding to a strong variation in organic matter productivity, with the Upper and Lower LCG members having much higher organic matter productivities than the Middle LCG Member.

Volcanic ash can fertilize surface water and enhance primary productivity by releasing mineral ions such as iron in modern lakes and oceans (Langmann et al., 2010). Duggen et al. (2007) recognized that volcanic ash could stimulate phytoplankton and promote productivity based on biogeochemical experiments. With the discovery of a large amount of tight oil and shale oil in the Jimsar Sag, a lot of research has been carried out on reservoir characteristics (Zhang et al., 2019; Yang et al., 2019; Pan et al., 2020; Lin et al., 2021), especially microscopic characteristics. It was found that large amounts of volcanic material were deposited in the LCG Formation, including volcanic extrusive rock debris, euhedral lath-shaped and acicular crystal form plagioclase (Zhang et al., 2019), and tuff rock fragments (Lin et al., 2021). Ankerite and analcime, which may be related to frequent volcanic activity, were also were discovered in the LCG Formation (Pan et al., 2020; Zhang et al., 2019). Evidence from rare earth elements indicate that the formation of the dolomite had a relationship with the existing volcanic materials (Yang et al., 2019; Lin et al., 2021). Therefore, the higher organic matter production of the Upper and Lower members may be related to the presence of volcanic ash. It was volcanic ash that promoted the organic matter production of Lower and Upper LCG

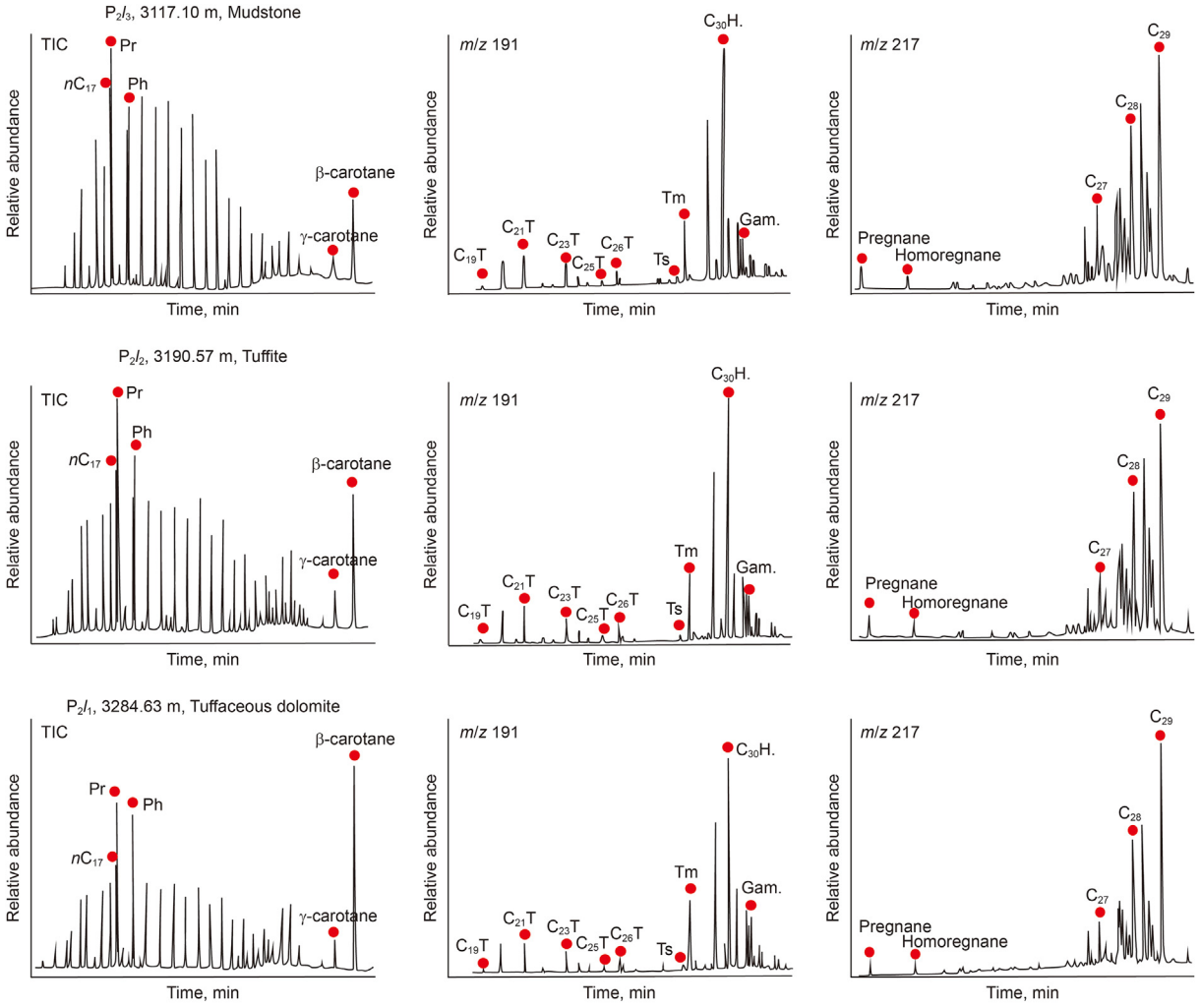

Fig. 7. Representative mass chromatograms of TIC, terpane (m/z = 191) and sterane (m/z = 217) series of saturate fractions for different lithology within the Lower Permian Lucaogou Formation in the Jimsar Sag of the Junggar Basin. Pr = pristine; Ph = phytane; $C_{19}T$ = C_{19} tricyclic terpane; $C_{21}T$ = C_{21}tricyclic terpane; $C_{23}T$ = C_{23}tricyclic terpane; $C_{25}T$ = C_{25}tricyclic terpane; Ts = 18α (H)-22, 29, 30- trisnorneohopane; Tm = 17α(H)-22,29,30-trisnorhopane; $C_{30}H$ = C_{30}hopane; Gam. = Gammacerane; C_{27} = C_{27}sterane 20R; C_{28} = C_{28}sterane 20R; C_{29} = C_{29}sterane 20R.

members and caused strong heterogeneity.

5.3. Depositional environment and the preservation of organic matter

The preservation of organic matter depends on the depositional environment, especially the redox conditions (Demaison and Moore, 1980; He et al., 2022), which can be often characterized by pristane/phytane (Pr/Ph) ratio. A Pr/Ph ratios of less than 1 indicates a reducing environment (sub-oxic or anoxic), while the ratios of greater than 1 indicate oxidizing conditions (Didyk et al., 1978). As illustrated in Fig. 12 and Appendix Table 3, the Pr/Ph ratio in the study area ranges for the Upper, Middle and Lower LCG members are 1.03–2.1 (average 1.33), 0.94–1.5 (average 1.23), and 0.74–1.45 (average 1.03), respectively, corresponding to a weakly oxidizing (Middle and Upper LCG members) to weakly reducing (Lower LCG Member) depositional environments (Fig. 12). Although there is a positive correlation between Pr/Ph ratio and thermal maturity (Connan, 1973; Albrecht et al., 1976), our study demonstrates that Pr/Ph ratio is not controlled by thermal maturity.

The redox conditions of the Lucaogou Formation deduced from the Pr/Ph ratio are consistent with the results from Pr/nC_{17} vs. Ph/nC_{18} plot (Fig. 13; Peters et al., 1999). The Pr/n-C_{17} ratio of the samples varies between 0.14 and 2.25, and the Ph/n-C_{18} ratio between 0.09 and 3.08 (Appendix Table 3), with most of the data from the Lower LCG Member plotted in the reducing region and most of the data from the Middle and Upper LCG members plotted in the weaking oxidizing region in Fig. 13.

In addition to Pr/Ph ratio, the ratio of $C_{35}22S/C_{34}22S$ hopane is also an effective indicator of redox condition (Peters and Moldowan, 1991). The Lower LCG Member with the relatively low Pr/Ph ratios has relatively high $C_{35}22S/C_{34}22S$ ratios, while the Middle and Upper LCG members with the relatively high Pr/Ph ratios have relatively low $C_{35}22S/C_{34}22S$ ratios (Table 3, Fig. 13). Accordingly, it is reasonable to assume that weak reducing conditions prevailed in the bottom water during the deposition of the Lower LCG Member, and to the contrary, weak oxidizing conditions were predominant in the bottom water in lakes during the deposition of the Middle and Upper LCG members.

Gammacerane is derived from bacterivorous ciliates which generally live at the interface of stratified water columns (Damsté et al., 1995). Both hypersalinity and temperature gradient could give rise to stratification (Bohacs et al., 2000), but high abundances of gammacerane are mostly found in hypersaline environments

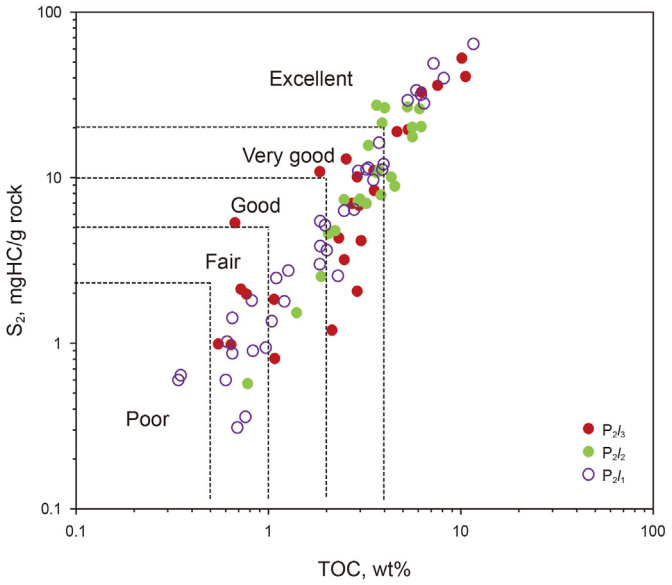

Fig. 8. Total organic carbon (TOC) contents versus Rock-Eval S_2 peaks (mg hydrocarbons [HC]/g rock) for shale samples from the Lucaogou Formation (P_2l) of the Jimsar Sag.

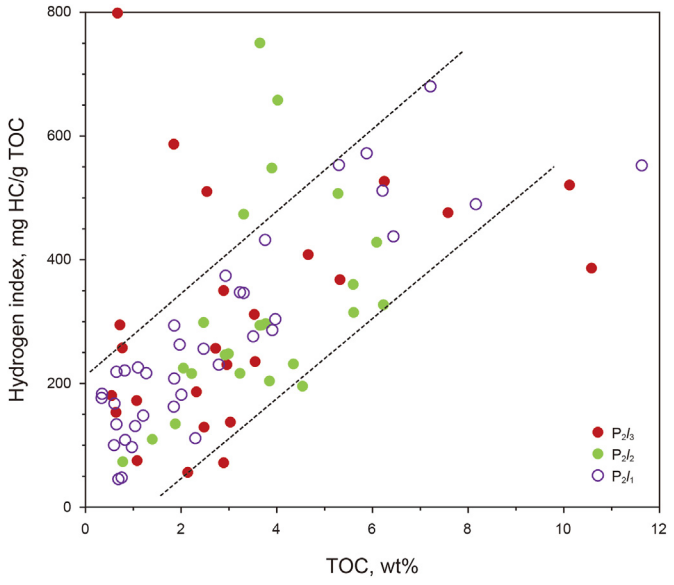

Fig. 10. Plot of Hydrogen Index versus TOC, showing the positive correlation between hydrogen index and TOC of the Lucaogou Formation in the Jimsar Sag of the Junggar Basin.

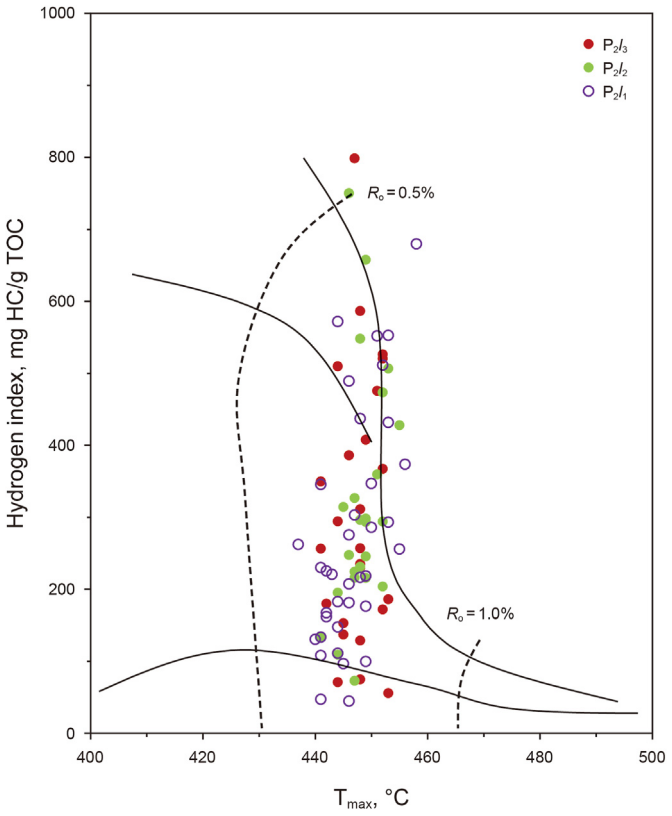

Fig. 9. Plot of Hydrogen Index versus T_{max} outlining the kerogen type of the Lucaogou Formation in the Jimsar Sag of the Junggar Basin.

(Summons et al., 2008). The gammacerane index (gammacerane/C_{30}hopane) of the LCG Formation samples ranges from 0.05 to 0.27, which probably indicates a fresh to brackishwater environment and unstable water column stratification (Table 3 and Fig. 12). The extended tricyclic terpane ratio [ETR = $(C_{28} + C_{29})/(C_{28} + C_{29} + Ts)$] also is an effective indicator of the salinity during or immediately after the deposition of source sediments in the Junggar Basin (Hao et al., 2009). The ETR of the source rock samples is between 0.22 and 0.83 (Table 3), and its vertical distribution follows a similar trend as the gammacerane index (Fig. 12). Salinity of the LCG Formation is small, e.g., from the bottom to the top of LCG Formation, salinity first decreases slightly and then increases.

The redox condition of the depositional environment is one of the main factors controlling the preservation of organic matter. Organic-rich deposits are thought to be associated primarily with anoxic settings (Demaison and Moore, 1980; Hedges and Keil, 1995). Manganese reduction, nitrate reduction, iron reduction, bacterial sulfate reduction and methane fermentation all cause degradation of organic matter and affect organic matter preservation (Fike et al., 2006; Roberts, 2015). Among them, bacterial sulfate reduction (BSR), in a reducing deposition environment, has much stronger oxidation capacity than other oxidizers, such as oxygen, nitrate, and metallic oxide (Reeburgh, 1980). In a coastal sea-bed, BSR can degrade more than half of the organic matter (Jørgensen, 1982). On the other hand, in a freshwater lake, BSR has a less effect on organic matter due to low sulfate concentration. However, in salt lakes with high sulfate concentrations, e.g., from the influx of volcanic ash or thermal fluid (Davison, 1988), organic matter abundance of sediments is usually low because of BSR effect (Kelts, 1988).

One of the main products of BSR is framboidal pyrite (Berner and Raiswell, 1983; Berner, 1984; Raiswell and Berner, 1985). Most pyrite in the LCG organic-matter-rich sediments has a framboidal shape (Fig. 4), with pyrite content ranging from 0.4% to 11.0% (Appendix Table 1; Fig. 12). Based on the pyrite content, the BSR effect of organic matter in the Lower LCG Member is high, in the Upper LCG and Middle members is low. Furthermore, Xie et al. (2015) found suspected sulfate reducing bacteria in the LCG Formation of the Jimsar Sag. It is indicated that there was a certain content of sulfate in the LCG deposition and bacteria sulfate reduction occurred.

In order to define the degree of BSR, Lallier-Vergès et al. (1993a, 1993b) defined the sulfate reduction index (SRI). SRI could be calculated from the following equation:

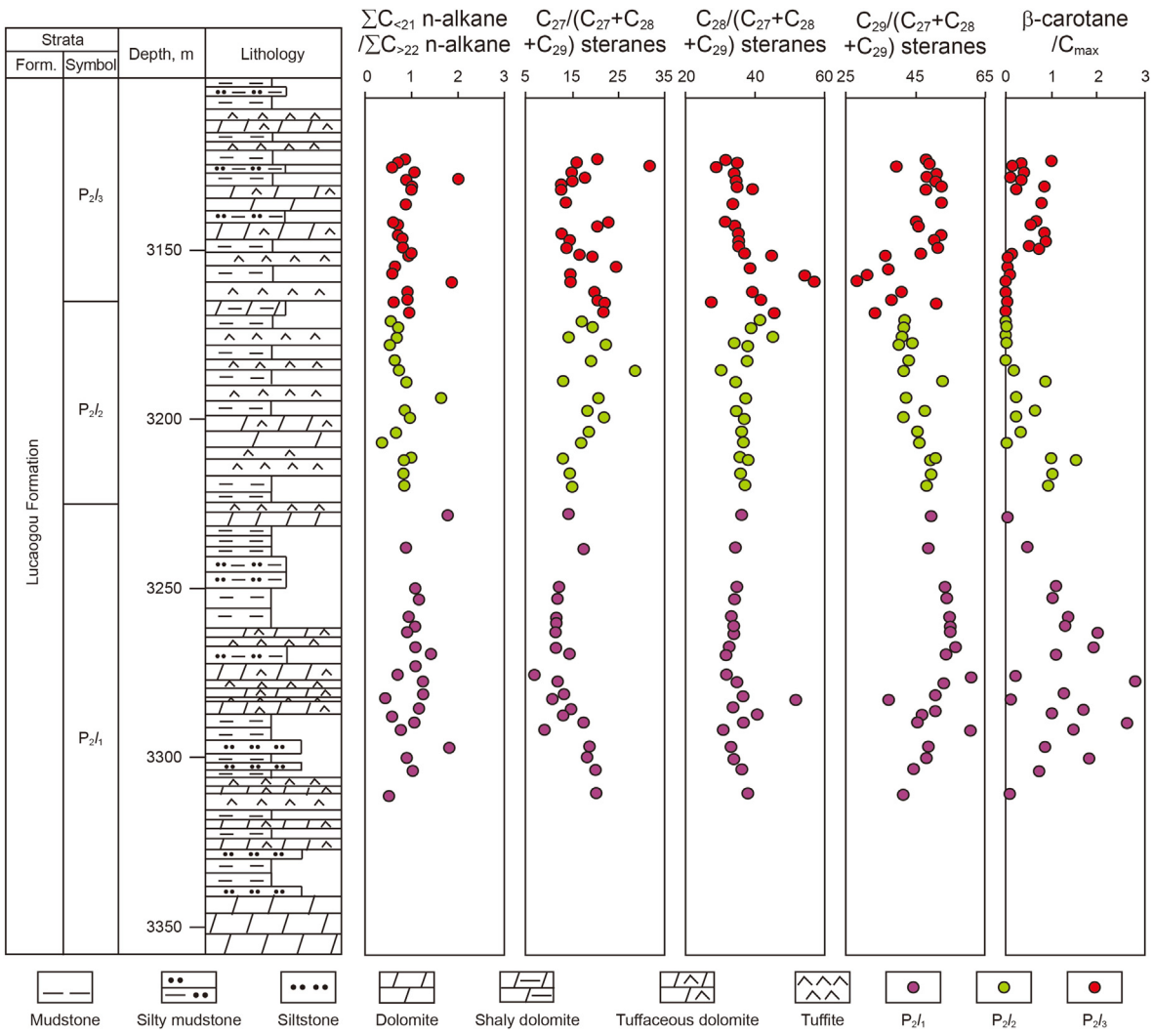

Fig. 11. Composite organic geochemistry profile showing changes in major biomarker parameters and stable carbon isotopes of carbonate, reflecting organic matter input of LCG sediments. Abbreviations for biomarker parameters are explained in Table 3. The stable carbon isotope of carbonate data is from Wu et al. (2017).

$$SRI = (TOC + TS / 1.33) / TOC = 1 + 0.75 \times TS / TOC$$

TS represents total sulfur of organic matter. The SRI reflects the degree of the BSR, and the higher BSR degree, the higher SRI value. For instance, Liu et al. (2021) and Li et al. (2021) have used SRI to analyze the role of BSR played in organic matter preservation. According to SRI of LCG (Fig. 12), the degree of BSR in the Lower LCG Member is high, and in the Upper and Middle LCG member are low, which is consistent with the pyrite content.

5.4. Factors controlling accumulation of organic matter

Organic matter accumulation is a very complex process controlled predominantly by production and preservation of organic matter (Pedersen and Calvert, 1990; Arthur and Dean, 1998; Katz, 2005). Other controlling factors include climate, water chemistry, weather and tectonic setting.

5.4.1. The lower LCG member

The Lower LCG Member is dominated by dolomite, tuffaceous dolomite and mudstone. In the Lower LCG Member, both TOC content (0.34%–11.63%) and HI (45–680 mg/gTOC) show very strong heterogeneity and similar vertical distribution (Fig. 14). Phytoplankton and aquatic algal-bacterial organisms, especially cyanobacteria, were the main source of the organic matter in the Lower LCG Member, which can be inferred from high proportion of C_{29} steranes (29%) and relatively high content of β-carotane. The Pr/Ph ratio has a range of 0.74–1.45 and a mean value of 1.03, representing a relatively weak reducing depositional environment. So it could be asserted that organic matter degradation by oxygen was limited. The extent of BSR is strong, which is suggested by the high content of framboidal pyrite and SRI value (Fig. 12).

As supported by the negative correlation between TOC and pyrite content (Fig. 14), BSR is the main factor controlling the degradation and accumulation of organic matter. Where the core samples have a relatively higher TOC content, the pyrite content is usually lower, as in sections “B”, “D” and “F”. While, sections “A”, “C”, and “E” have relatively low TOC content with relatively high pyrite. In addition, production and preservation of organic matter also influence organic matter accumulation. For example, the above-mentioned section “B” and “D” have relatively higher TOC content and β-carotane than section “F” (Fig. 14).

The accumulation of organic matter is controlled by the source, production, and preservation of organic matter. For the Lower LCG Member, the preservation of organic matter is the main controlling factor for the accumulation of organic matter, which, in turn, is

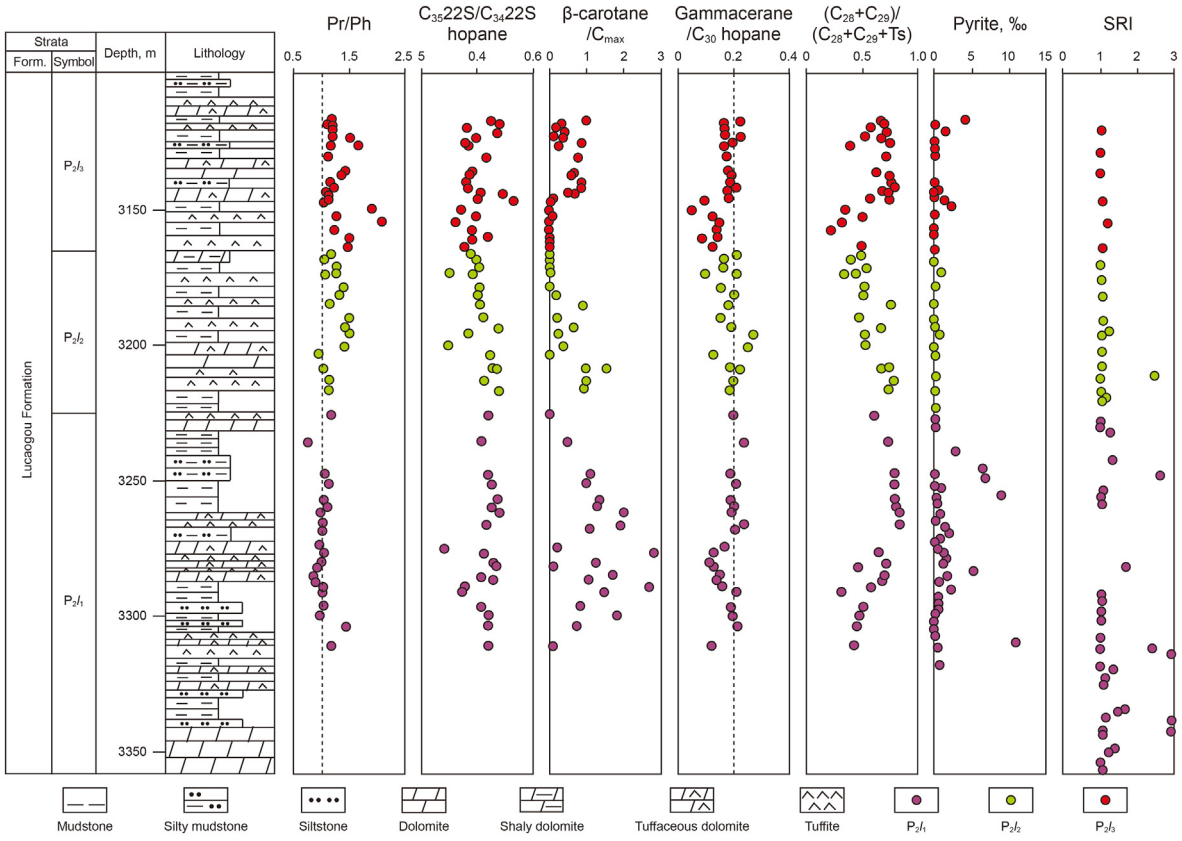

Fig. 12. Composite organic geochemistry profile showing changes in major biomarker parameters and pyrite content of LCG sediments, reflecting depositional conditions and organic matter preservation. Abbreviations for biomarker parameters are explained in Table 3.

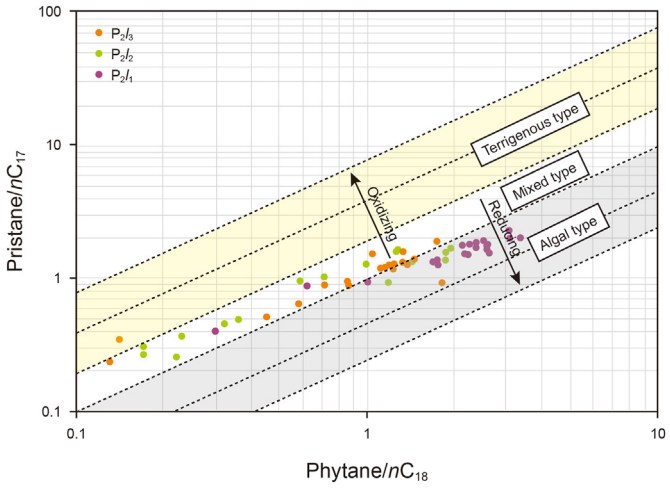

Fig. 13. Relationship between Ph/nC_{18} and Pr/nC_{17} ratio values for the shale within the Lower Permian Lucaogou Formation in the Jimsar Sag of the Junggar Basin (modified after Peters et al., 1999).

determined by the degree of BSR.

5.4.2. Middle LCG formation

Compared to the Lower LCG Member, the Middle LCG Member is dominated by carbonate rocks with little influx of volcanic ash (Fig. 15). The TOC content and HI are 0.78%–6.23% and 73–750 mg/g TOC, with mean values of 3.65% and 319 mg/g TOC, respectively. The Pr/Ph ratio shows that its redox condition is weak reducing to weak oxidizing in section "G" and weak oxidizing in section "H". Because of a lack of volcanic ash and low sulfate concentration during deposition, there was almost no organic matter degradation by BSR, which is consistent with the very low pyrite content and low SRI value (Fig. 12). In other words, the organic matter preservation in the Middle LCG Member is mainly controlled by redox condition other than BSR.

Both the TOC and C_{27} steranes tend to increase in section "G" and then decrease in section "H", while C_{29} steranes (29%) and β-carotane decrease from the bottom to the top in the Middle LCG Member (Fig. 15). Therefore, the organic matter accumulation is mainly controlled by the productivity represented by the proportion of C_{27} steranes, not C_{29} steranes (29%) and β-carotane. It is noteworthy that the samples of the upper part of section "G" have much higher C_{27} steranes but not much higher TOC content compared to the lower part. This is likely to have been a result of oxidizing depositional environment where partial degradation of organic matter took place.

The accumulation of organic matter in the Middle LCG Member is mainly controlled by productivity, which is represented by the proportion of C_{27} steranes. The preservation of organic matter, determined by redox condition, also played a role on the accumulation of the organic matter. Due to a generally oxidizing redox condition and low sulfate concentration, BSR has a weak effect on the preservation and accumulation of organic matter.

5.4.3. The upper LCG member

In the Upper LCG Member, both TOC content and HI show significant variations, with a range of 0.55%–10.58% and 56–798 mg/g TOC, respectively (Fig. 16). The Pr/Ph ratio ranges from 1.07 to 2.1,

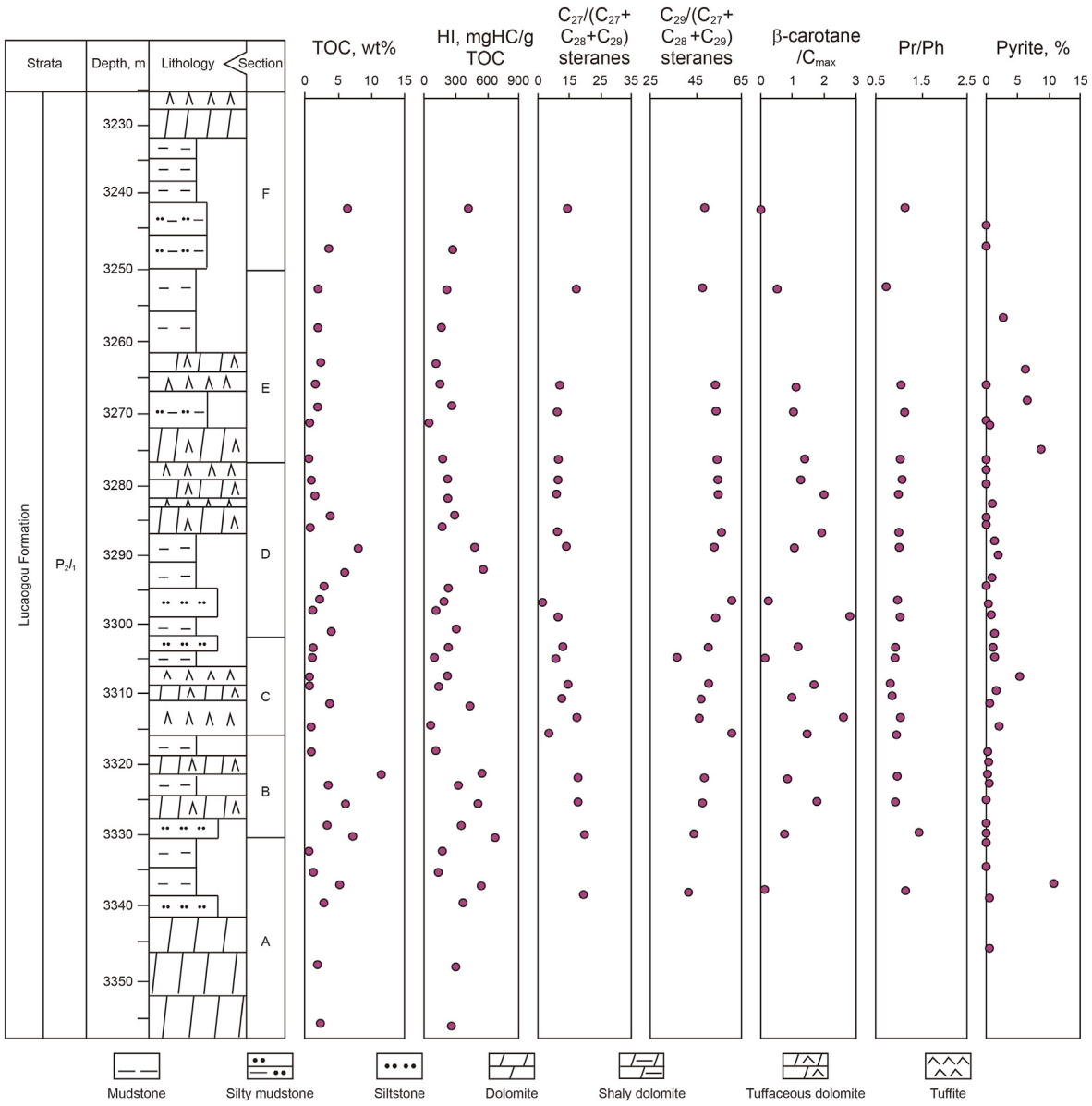

Fig. 14. Composite organic geochemistry profile showing changes in TOC, HI, pyrite content and major biomarker parameters reflecting organic matter abundance, type, depositional conditions and organic matter input of the Lower LCG shale. Abbreviations for biomarker parameters are explained in Tables 2 and 3.

with average of 1.33, indicating a relatively weak oxidizing depositional environment and degradation of organic matter mainly by oxygen. The low pyrite content and low SRI value indicate that degradation by BSR is rare.

The TOC content and C_{27} steranes (27%) have a similar variation trend (Fig. 16). For example, core samples with high TOC also have high proportion of C_{27} steranes. Thus, the accumulation of organic matter is mainly controlled by productivity. The proportion of C_{27} steranes in section "I" is as high as that in section "J", but the TOC content in section "I" is much lower than that in "J". This is because in section "I", partial organic matter was degraded in an oxidizing depositional environment. In section "K", the proportion of C_{27} steranes is also as high as section "J", but the TOC content is lower than section "J". In a reducing depositional environment, degradation of organic matter by oxygen is limited in section "K".

Therefore, in the Upper LCG Member, the accumulation organic matter is mainly controlled by productivity of organic matter, especially the high concentrations of C_{27} steranes. The organic matter was mainly degraded by oxygen in an oxidizing depositional setting. The preservation of organic matter also played a minor role on the accumulation of organic matter.

5.5. Model of organic matter accumulation

During the deposition of LCG, the Jimsar Sag was characterized by a period of relative stability. The accumulation of organic matter of LCG organic-matter-rich shale was mainly controlled by productivity or preservation of organic matter, which can be partly attributed to input of volcanic ash. In order to fully demonstrate the organic matter accumulation process, two models for the accumulation of organic matter were proposed for the LCG Formation based on the comprehensive analysis of organic matter origin, production, depositional environment, and preservation of organic matter.

In model A (Fig. 17), the high influx of volcanic ash released nutrients, such as nitrate and iron, causing cyanobacteria to bloom

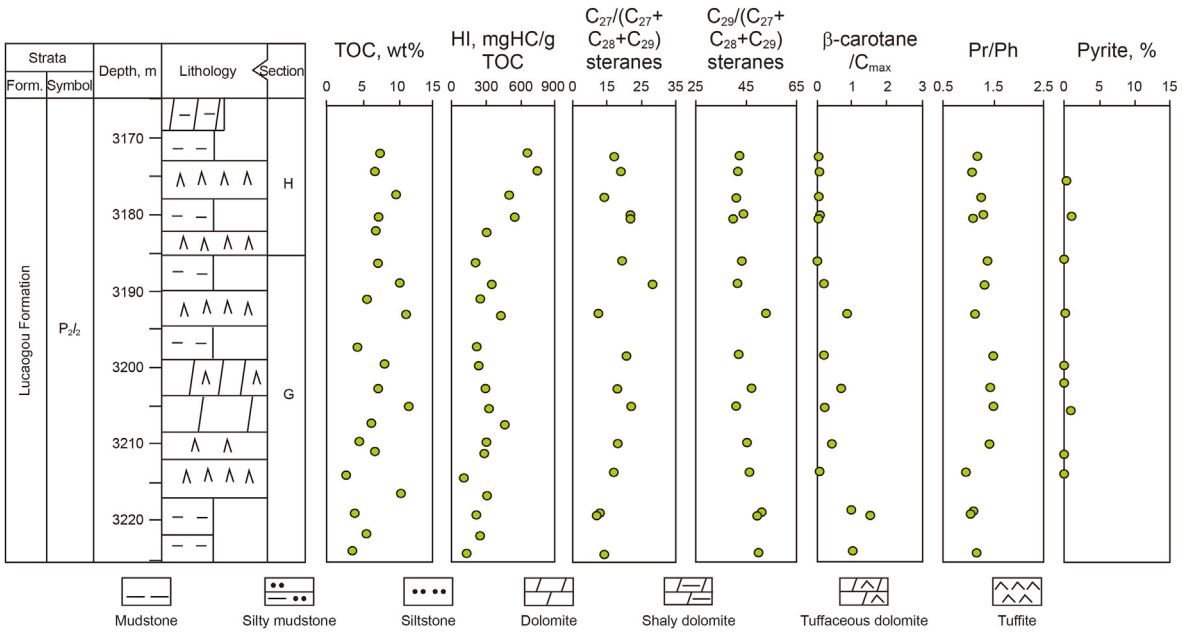

Fig. 15. Composite organic geochemistry profile showing changes in TOC, HI, pyrite content and major biomarker parameters reflecting organic matter abundance, type, depositional conditions and organic matter input of the Middle LCG shale. Abbreviations for biomarker parameters are explained in Tables 2 and 3.

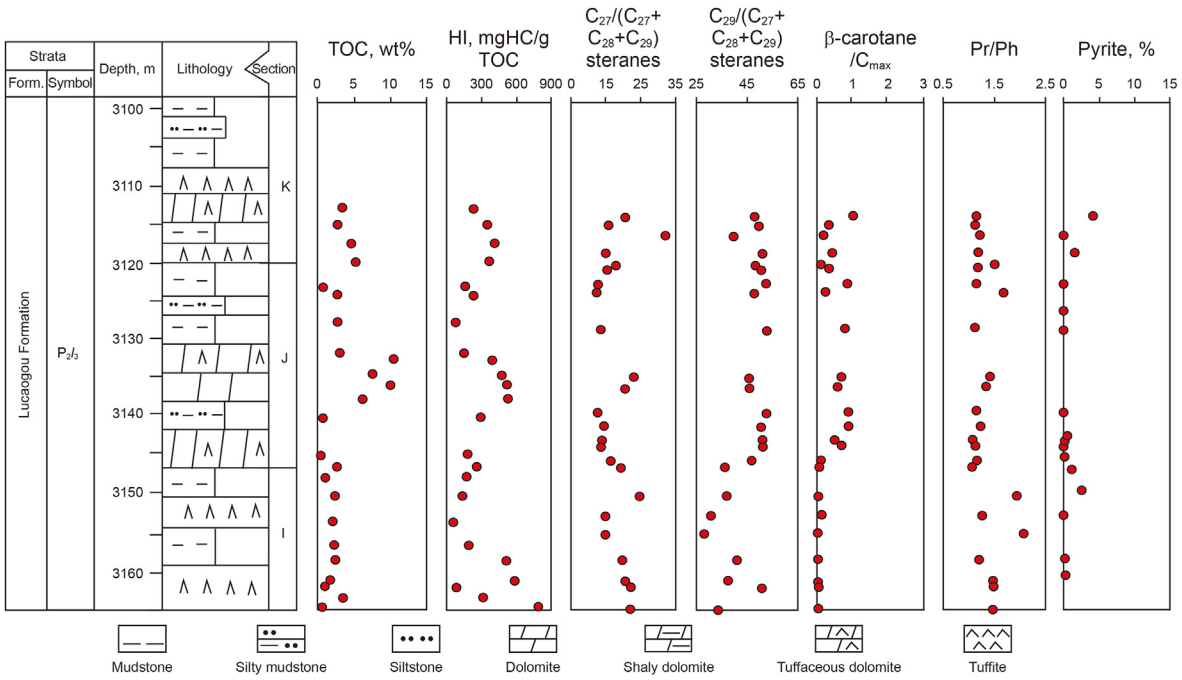

Fig. 16. Composite organic geochemistry profile showing changes in TOC, HI, pyrite content and major biomarker parameters reflecting organic matter abundance, type, depositional conditions and organic matter input of the Upper LCG shale. Abbreviations for biomarker parameters are explained in Tables 2 and 3.

and high productivity. This is suggested by the high content of C_{29} steranes and β-carotane. The volcanic ash also brought abundant sulfate into the water, leading to bacterial sulfate reduction (BSR) and framboidal pyrite formation. In this model, the accumulation of organic matter is mainly controlled by the preservation of organic matter, which is mainly controlled by BSR not oxygen content due to the reducing depositional environment. Model A is used to explain the accumulation of organic matter in the Lower LCG Member, such as the Section "B", "D", and "F" (Fig. 14). Elevated production of organic matter played a minor role on the accumulation of organic matter in this model.

In the model B, the influx of volcanic ash was small and did not induce a cyanobacteria bloom. The production of organic matter was mainly phytoplankton (Fig. 17). Due to the low sulfate and the

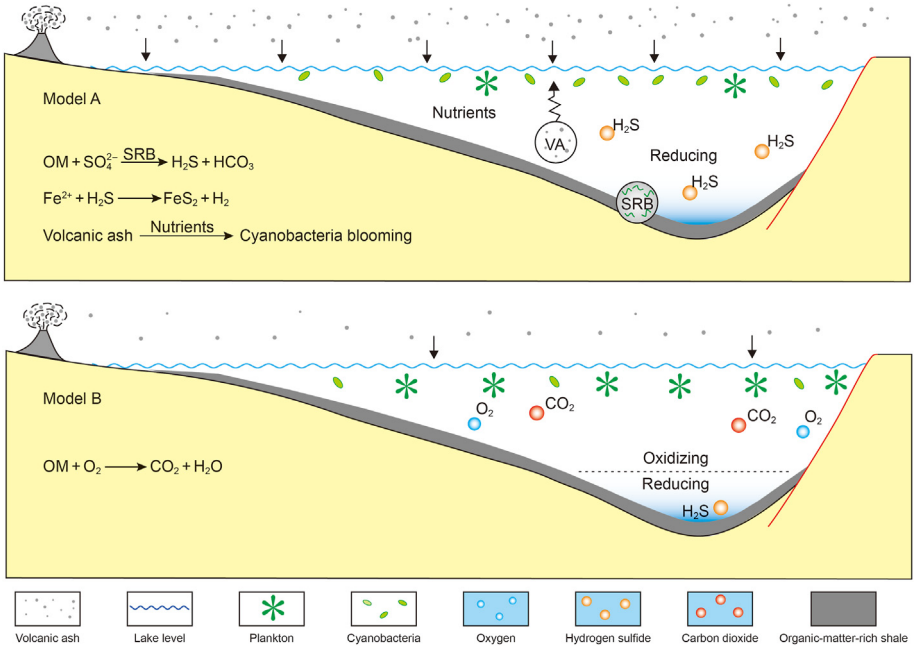

Fig. 17. Organic matter accumulation model of the LCG organic-matter-rich shale in the Jimsar Sag, Junggar Basin. OM, organic matter; VA, volcanic ash; SRB, sulfate reducing bacteria.

weak BSR, organic matter was mainly degraded by oxygen and controlled by the redox condition of depositional environment. In model "B", the accumulation of organic matter is mainly determined by the production of organic matter while the preservation of organic matter has a minor effect. Model B is used to explain the accumulation process of organic matter in the Middle and Upper LCG members. In an oxidizing depositional environment, such as in the upper part of section "G" of the Middle LCG Member, part of organic matter was mainly degraded by oxygen (Fig. 15). In a reducing depositional environment, such as in the Section K of the Upper LCG Member, part of organic matter was degraded by BSR (Fig. 16).

In summary, volcanic ash input and depositional environment led to the variance in the origin, production and preservation of organic matter in the LCG organic-rich shale in the Jimsar Sag. The accumulation of organic matter in the organic-rich shale can be explained by synergetic evolution of environments, organisms, and geological events in the lake systems through two different models.

6. Conclusions

Based on the mineralogy and microscopic study of organic matter, as well as bulk and molecular geochemical measurements of more than 200 core samples, the origin, production, depositional environment, preservation and accumulation of organic matter in the LCG Formation in the Jimsar Sag of the Junggar Basin was deduced. The following conclusions could be drawn.

The Lucaogou Formation in the Jimsar Sag contains carbonate, siliclastic and volcaniclastic material with a wide range of total organic carbon contents and hydrogen indices, indicating that they are good to excellent source rocks with high hydrocarbon generation potential. According to the comprehensive analysis of various biomarkers, the organic matter in the Lucaogou Formation mainly originated from phytoplankton and aquatic algal-bacterial organisms (cyanobacteria in particular). It appears that the volcanic ash promoted the cyanobacteria blooming and caused strong productivity.

Reducing conditions prevailed in the bottom water during the deposition of the Lower Lucaogou Member. The organic matter was mainly degraded by bacterial sulfate reduction. To the contrary, oxidizing conditions dominated in the bottom water in lakes during the deposition of Middle and Upper LCG members, and the organic matter was in general degraded by oxygen.

Volcanic ash played an essential role in promoting and suppressing organic matter accumulation of LCG shale through causing cyanobacteria blooming and bacterial sulfate reduction respectively. The synergetic evolution of environments, organisms, and geological events in the lake systems accounted for two different organic matter accumulation models in organic-matter-rich shale: "bacterial sulfate reduction controlling model" and "productivity model".

Acknowledgments

We thank the editor, B. J. Katz and another three anonymous reviewers for their insightful reviews, which greatly improved the article. This work was supported by National Science Foundation for Young Scientists of China (Grant 41702143), Major basic science and technology projects of CNPC (2021DJ0206-03). We also would like to thank Xinjiang Oil Field Company for providing the cored rock samples.

Appendix. Table

Appendix Table 1
X-ray Diffraction data of shale within the Permian Lucaogou Formation in the Jimsar Sag, Junggar Basin

Depth, m	Quartz, %	Plagioclase, %	K-feldspar, %	Clay, %	Dolomite, %	Ankerite, %	Calcite, %	Pyrite, %	Hematite, %	Siderite, %	Zeolite, %	Laumontite, %
3112.09	39.30	20.60	6.00	11.60	18.40	0.00	0.00	4.10	0.00	0.00	0.00	0.00
3114.86	18.40	26.90	3.20	2.40	49.10	0.00	0.00	0.00	0.00	0.00	0.00	0.00
3116.94	29.20	45.90	5.90	2.20	15.30	0.00	0.00	1.50	0.00	0.00	0.00	0.00
3121.38	8.20	11.10	0.60	0.00	80.10	0.00	0.00	0.00	0.00	0.00	0.00	0.00
3124.97	21.10	22.40	5.80	10.60	24.00	0.00	16.10	0.00	0.00	0.00	0.00	0.00
3127.53	27.90	45.30	13.10	8.80	0.00	0.00	2.70	0.00	0.00	2.20	0.00	0.00
3138.76	11.60	10.60	0.70	0.90	76.20	0.00	0.00	0.00	0.00	0.00	0.00	0.00
3142.13	14.00	49.80	2.00	3.10	0.00	14.30	16.30	0.50	0.00	0.00	0.00	0.00
3142.77	12.80	14.90	1.60	2.40	67.50	0.00	0.80	0.00	0.00	0.00	0.00	0.00
3143.64	16.10	47.20	2.70	2.30	0.00	29.50	2.20	0.00	0.00	0.00	0.00	0.00
3144.84	25.50	43.90	4.50	5.60	20.50	0.00	0.00	0.00	0.00	0.00	0.00	0.00
3146.54	14.60	15.10	3.80	9.80	53.70	0.00	1.80	1.20	0.00	0.00	0.00	0.00
3149.6	33.00	22.80	7.90	13.20	0.00	9.70	10.70	2.70	0.00	0.00	0.00	0.00
3152.82	15.70	10.60	1.80	1.80	70.10	0.00	0.00	0.00	0.00	0.00	0.00	0.00
3158.68	27.30	44.70	4.70	14.70	0.00	5.30	3.30	0.00	0.00	0.00	0.00	0.00
3160.99	16.80	18.00	1.80	11.70	51.70	0.00	0.00	0.00	0.00	0.00	0.00	0.00
3167.94	28.70	27.00	4.70	14.10	0.00	25.50	0.00	0.00	0.00	0.00	0.00	0.00
3172.58	20.10	4.10	0.50	1.70	48.20	0.00	25.40	0.00	0.00	0.00	0.00	0.00
3177.34	22.60	42.40	4.40	8.80	16.70	0.00	4.20	0.90	0.00	0.00	0.00	0.00
3183.36	20.30	7.00	0.00	0.00	71.40	0.00	1.30	0.00	0.00	0.00	0.00	0.00
3190.64	23.10	15.40	2.70	11.70	47.10	0.00	0.00	0.00	0.00	0.00	0.00	0.00
3197.79	9.00	4.30	0.00	6.80	60.10	0.00	19.80	0.00	0.00	0.00	0.00	0.00
3199.99	22.50	46.60	3.90	5.90	0.00	7.70	13.40	0.00	0.00	0.00	0.00	0.00
3203.85	29.90	15.60	2.40	24.00	1.90	0.00	5.00	0.70	0.00	0.00	20.50	0.00
3209.61	21.00	29.20	3.70	17.50	28.60	0.00	0.00	0.00	0.00	0.00	0.00	0.00
3212.43	22.20	21.30	7.00	35.90	0.00	4.90	8.70	0.00	0.00	0.00	0.00	0.00
3221.79	22.20	25.80	4.50	13.00	20.10	0.00	14.40	0.00	0.00	0.00	0.00	0.00
3227.98	31.60	28.10	6.70	11.50	22.10	0.00	0.00	0.00	0.00	0.00	0.00	0.00
3235.05	18.50	28.60	7.00	23.20	0.00	3.50	18.40	0.00	0.80	0.00	0.00	0.00
3240.22	16.40	17.10	2.30	12.30	43.10	0.00	8.80	0.00	0.00	0.00	0.00	0.00
3243.23	23.30	33.40	3.20	11.20	0.00	21.10	7.80	0.00	0.00	0.00	0.00	0.00
3253.56	15.90	23.50	5.30	14.50	18.50	0.00	19.50	2.80	0.00	0.00	0.00	0.00
3261.23	11.20	27.70	2.00	5.80	45.50	0.00	1.50	6.30	0.00	0.00	0.00	0.00
3263.36	24.60	32.00	5.80	8.10	28.80	0.00	0.70	0.00	0.00	0.00	0.00	0.00
3265.56	18.80	8.90	1.20	2.90	61.00	0.00	0.10	7.10	0.00	0.00	0.00	0.00
3268.48	26.30	34.00	3.80	9.40	26.50	0.00	0.00	0.00	0.00	0.00	0.00	0.00
3269.07	16.80	24.10	2.70	7.20	48.50	0.00	0.00	0.70	0.00	0.00	0.00	0.00
3272.6	29.50	9.00	12.20	14.10	0.00	3.30	23.00	8.90	0.00	0.00	0.00	0.00
3273.95	14.50	23.70	4.90	2.10	54.80	0.00	0.00	0.00	0.00	0.00	0.00	0.00
3275.43	15.80	32.50	4.90	5.90	40.10	0.00	0.50	0.30	0.00	0.00	0.00	0.00
3277.5	15.60	25.40	4.40	6.00	48.60	0.00	0.00	0.00	0.00	0.00	0.00	0.00
3280.74	21.40	36.30	5.50	7.30	11.70	0.00	16.90	0.90	0.00	0.00	0.00	0.00
3282.63	24.80	26.50	10.40	14.80	23.50	0.00	0.00	0.00	0.00	0.00	0.00	0.00
3283.38	17.50	40.10	4.90	12.40	17.70	0.00	7.40	0.00	0.00	0.00	0.00	0.00
3283.74	20.30	45.20	3.90	6.10	23.50	0.00	1.00	0.00	0.00	0.00	0.00	0.00
3285.81	21.60	42.20	5.20	5.80	23.80	0.00	0.00	1.40	0.00	0.00	0.00	0.00
3288.27	14.30	12.90	1.20	7.60	25.50	0.00	36.60	1.90	0.00	0.00	0.00	0.00
3291.24	20.10	25.30	3.80	11.40	38.60	0.00	0.00	0.80	0.00	0.00	0.00	0.00
3292.49	22.20	19.90	2.20	10.50	45.20	0.00	0.00	0.00	0.00	0.00	0.00	0.00
3295.24	19.50	17.20	4.40	12.50	37.30	0.00	8.70	0.40	0.00	0.00	0.00	0.00
3296.61	20.70	19.90	4.20	8.40	45.60	0.00	0.20	1.00	0.00	0.00	0.00	0.00
3299.1	12.80	17.70	1.20	10.30	0.00	14.40	42.10	1.50	0.00	0.00	0.00	0.00
3301.42	16.90	17.10	4.30	12.70	46.10	0.00	1.70	1.20	0.00	0.00	0.00	0.00
3302.68	17.10	29.10	5.20	15.40	17.00	0.00	14.80	1.40	0.00	0.00	0.00	0.00
3305.33	21.00	18.20	1.80	6.60	41.20	0.00	5.80	5.40	0.00	0.00	0.00	0.00
3307.28	24.80	18.30	7.20	24.20	0.00	21.00	2.90	1.60	0.00	0.00	0.00	0.00
3309.4	24.20	21.60	6.20	19.00	27.30	0.00	1.10	0.60	0.00	0.00	0.00	0.00
3312.59	18.00	31.20	6.50	19.30	7.50	0.00	15.20	2.30	0.00	0.00	0.00	0.00
3316.35	20.90	15.50	3.10	20.90	38.90	0.00	0.30	0.40	0.00	0.00	0.00	0.00
3318.01	26.60	17.40	5.00	20.50	13.40	0.00	16.60	0.50	0.00	0.00	0.00	0.00
3319.56	35.10	20.90	2.70	10.30	28.60	0.00	2.40	0.00	0.00	0.00	0.00	0.00
3320.91	29.30	18.70	2.30	15.10	33.20	0.00	0.80	0.60	0.00	0.00	0.00	0.00
3323.38	9.00	3.00	0.00	3.60	0.00	0.00	84.40	0.00	0.00	0.00	0.00	0.00
3326.83	31.90	26.80	6.40	15.00	19.90	0.00	0.00	0.00	0.00	0.00	0.00	0.00
3327.94	16.70	6.70	1.10	12.50	44.10	0.00	18.90	0.00	0.00	0.00	0.00	0.00
3329.68	13.10	5.00	0.70	7.50	13.50	0.00	60.20	0.00	0.00	0.00	0.00	0.00
3332.81	30.70	11.10	4.40	24.50	23.60	0.00	5.70	0.00	0.00	0.00	0.00	0.00
3335.41	10.10	9.80	1.30	10.80	8.00	0.00	41.10	11.00	0.00	0.00	7.90	0.00
3337.43	16.30	9.80	2.10	11.70	24.70	0.00	35.00	0.40	0.00	0.00	0.00	0.00
3344.75	25.90	11.60	2.20	27.70	0.00	0.00	25.90	0.60	0.00	0.00	6.10	0.00

Appendix Table 2
Total organic carbon and Rock-Eval pyrolysis data for shale within the Permian Lucaogou Formation in the Jimsar Sag, Junggar Basin.

Depth, m	TOC, %	S_1, mg/g	S_2, mg/g	T_{max}, °C	S_1+S_2, mg/g	HI, mg/g	Remark
3110.88	3.55	0.66	8.35	448	9.01	235.21	※
3113.3	2.89	1.96	10.11	441	12.07	349.83	※
3115.87	4.66	0.49	19.00	449	19.49	407.73	
3118.33	5.32	0.29	19.55	452	19.84	367.48	
3121.68	0.64	0.05	0.98	445	1.03	153.13	
3122.87	2.96	0.54	6.81	448	7.35	230.07	
3126.61	2.89	1.00	2.06	444	3.06	71.28	
3130.76	3.03	0.40	4.16	445	4.56	137.29	
3131.65	10.58	0.73	40.86	446	41.59	386.20	
3133.64	7.58	0.54	36.06	451	36.6	475.73	
3135.11	10.12	0.93	52.68	452	53.61	520.55	
3137.01	6.25	0.36	32.9	452	33.26	526.40	
3139.70	0.72	0.03	2.12	444	2.15	294.44	
3144.66	0.55	0.06	0.99	442	1.05	180.00	※
3146.16	2.72	0.79	6.98	441	7.77	256.62	※
3147.68	1.07	0.12	1.84	452	1.96	171.96	
3150.20	2.48	0.64	3.20	448	3.84	129.03	
3153.65	2.14	0.12	1.20	453	1.32	56.07	
3156.94	2.32	0.15	4.32	453	4.47	186.21	
3158.88	2.54	0.24	12.95	444	13.19	509.84	
3161.75	1.85	0.02	10.85	448	10.87	586.49	※
3162.62	1.08	0.15	0.81	448	0.96	75.00	※
3164.06	3.53	0.32	10.99	448	11.31	311.33	
3165.32	0.67	0.05	5.35	447	5.4	798.51	
3166.74	0.77	0.54	1.98	448	2.52	257.14	
3168.69	4.02	0.4	26.44	449	26.84	657.71	
3171.29	3.65	0.3	27.38	446	27.68	750.14	
3174.40	5.28	0.75	26.76	453	27.51	506.82	
3177.55	3.90	0.26	21.37	448	21.63	547.95	※
3179.37	3.69	0.32	10.86	452	11.18	294.31	
3183.80	3.85	0.22	7.85	452	8.07	203.90	※
3186.56	5.60	1.18	20.14	451	21.32	359.64	
3188.62	2.92	0.36	7.18	449	7.54	245.89	
3190.88	6.09	0.47	26.07	455	26.54	428.08	
3195.18	2.22	1.17	4.79	449	5.96	215.77	
3197.57	4.35	0.29	10.06	448	10.35	231.26	
3200.90	3.77	0.33	11.18	448	11.51	296.55	
3203.56	6.23	1.51	20.36	447	21.87	326.81	
3205.67	3.31	0.42	15.67	452	16.09	473.41	
3208.16	2.47	0.45	7.37	449	7.82	298.38	
3209.61	3.65	0.27	10.72	449	10.99	293.70	
3212.87	1.40	0.11	1.53	444	1.64	109.29	
3215.32	5.61	1.02	17.64	445	18.66	314.44	
3217.98	2.05	0.36	4.60	447	4.96	224.39	
3220.85	2.99	3.01	7.41	446	10.42	247.83	
3223.23	1.88	1.31	2.53	441	3.84	134.57	
3227.14	3.23	1.09	6.98	447	8.07	216.10	※
3229.18	4.54	1.41	8.87	444	10.28	195.37	
3234.19	0.78	0.28	0.57	447	0.85	73.08	
3237.77	6.44	0.61	28.16	448	28.77	437.27	
3243.6	3.51	3.79	9.68	446	13.47	275.78	
3249.31	1.86	0.73	3.86	446	4.59	207.53	
3254.94	1.85	2.07	3.00	442	5.07	162.16	
3260.25	2.3	2.14	2.56	444	4.7	111.30	
3263.19	1.21	0.04	1.79	444	1.83	147.93	※
3266.32	1.97	3.00	5.17	437	8.17	262.44	
3268.81	0.69	0.01	0.31	446	0.32	44.93	
3273.95	0.35	0.01	0.64	444	0.65	182.86	
3276.99	0.82	0.01	1.81	443	1.82	220.73	※
3279.57	1.27	0.02	2.75	448	2.77	216.54	
3282.14	3.91	6.04	11.19	450	17.23	286.19	
3283.74	0.61	0.02	1.02	442	1.04	167.21	※
3286.70	8.16	1.16	39.94	446	41.1	489.46	※
3290.10	5.88	1.15	33.63	444	34.78	571.94	
3292.49	2.79	2.40	6.42	441	8.82	230.11	
3294.48	2.01	0.75	3.65	446	4.4	181.59	
3295.85	0.83	0.04	0.90	441	0.94	108.43	
3298.64	3.97	1.93	12.05	447	13.98	303.53	
3301.19	1.10	0.43	2.48	442	2.91	225.45	
3302.68	0.97	0.34	0.94	445	1.28	96.91	
3305.33	0.65	0.03	1.42	449	1.45	218.46	※
3306.97	0.65	0.09	0.87	441	0.96	133.85	※
3309.40	3.76	0.39	16.24	453	16.63	431.91	※
3312.59	0.76	0.50	0.36	441	0.86	47.37	※

Appendix Table 2 (*continued*)

Depth, m	TOC, %	S_1, mg/g	S_2, mg/g	T_{max}, °C	S_1+S_2, mg/g	HI, mg/g	Remark
3316.35	0.60	0.41	0.60	449	1.01	100.00	
3319.35	11.63	2.34	64.20	451	66.54	552.02	
3320.91	3.31	4.39	11.45	441	15.84	345.92	
3323.82	6.21	1.47	31.76	452	33.23	511.43	
3326.83	3.23	6.02	11.21	450	17.23	347.06	
3328.48	7.21	0.96	49.03	458	49.99	680.03	
3330.38	0.34	0.14	0.60	449	0.74	176.47	
3333.76	1.04	2.71	1.36	440	4.07	130.77	
3335.41	5.30	0.22	29.3	453	29.52	552.83	
3338.10	2.93	0.55	10.95	456	11.50	373.72	
3347.14	1.86	0.81	5.46	453	6.27	293.55	
3355.65	2.47	0.54	6.32	455	6.86	255.87	

Note: TOC = Total organic carbon (wt%); S_1 (mg/g), the amount of hydrocarbon of free; S_2 (mg/g), the amount of hydrocarbon produced by the cracking of organic matter; T_{max} (°C), the temperature which corresponds to the maximum generation rate from kerogen cracking; HI (hydrogen indices) = S_2/TOC, mg/g. The datas remarked with ※ is from Ding X.J. et al. (2019).

Appendix Table 3
Biomarker parameters for shale within the Permian Lucaogou Formation in the Jimsar Sag, Junggar Basin.

Depth, m	Pr/Ph	Pr/nC_{17}	Ph/nC_{18}	21−/22+	β/C_{max}	27%	28%	29%	20S, %	ββ, %	G/H	Ts/Tm	ETR	C_{35}/C_{34}	Remark
3112.09	1.17	1.17	1.11	0.85	1.00	20.53	31.45	48.02	0.39	0.26	0.22	0.11	0.67	0.45	※
3113.34	1.12	0.94	0.85	0.69	0.35	15.67	34.89	49.44	0.46	0.36	0.16	0.11	0.69	0.48	※
3114.73	1.21	1.21	1.18	0.57	0.16	31.83	28.72	39.45	0.36	0.21	0.17	0.16	0.57	0.36	※
3117.10	1.20	1.23	1.24	1.07	0.41	14.76	34.14	51.09	0.44	0.31	0.17	0.08	0.72	0.47	
3118.78	1.51	0.63	0.58	2.02	0.10	17.65	34.22	48.13	0.41	0.26	0.22	0.10	0.53	0.40	※
3119.23	1.18	0.90	1.80	0.87	0.35	14.93	34.28	50.78	0.45	0.35	0.16	0.11	0.68	0.39	※
3121.40	1.16	1.26	1.36	0.96	0.87	12.63	34.68	52.69	0.41	0.29	0.19	0.07	0.74	0.36	
3122.58	1.69	1.50	1.04	1.01	0.22	12.37	39.60	48.03	0.34	0.20	0.16	0.17	0.39	0.37	
3127.53	1.12	1.37	1.44	0.88	0.78	13.50	33.86	52.63	0.43	0.30	0.18	0.08	0.71	0.43	
3134.05	1.42	1.89	1.73	0.59	0.67	22.94	31.56	45.50	0.32	0.19	0.18	0.11	0.62	0.38	※
3135.31	1.35	1.59	1.33	0.72	0.56	20.25	34.09	45.66	0.38	0.26	0.19	0.07	0.75	0.37	
3138.76	1.15	1.18	1.23	0.72	0.87	12.53	35.28	52.19	0.42	0.29	0.19	0.07	0.75	0.36	
3140.71	1.22	1.36	1.36	0.83	0.87	14.44	35.04	50.52	0.38	0.26	0.21	0.06	0.78	0.37	
3142.65	1.07	1.19	1.15	0.78	0.49	13.76	35.09	51.15	0.43	0.28	0.17	0.08	0.69	0.41	
3143.30	1.13	1.30	1.32	0.82	0.69	13.43	35.24	51.33	0.44	0.28	0.18	0.07	0.73	0.49	
3145.44	1.16	0.87	0.86	1.03	0.10	16.41	36.67	46.92	0.40	0.26	0.18	0.09	0.56	0.40	
3146.19	1.03	0.50	0.45	0.93	0.03	19.22	44.60	36.19	0.32	0.17	0.09	0.13	0.74	0.53	※
3150.20	1.93	0.34	0.14	0.63	0.00	24.62	38.40	36.98	0.32	0.17	0.05	0.31	0.35	0.34	
3152.82	1.26	0.88	0.71	0.58	0.10	14.74	54.24	31.02	0.41	0.26	0.13	0.17	0.49	0.40	※
3155.32	2.10	0.20	0.09	1.88	0.00	14.69	57.26	28.05	0.31	0.19	0.15	0.18	0.32	0.32	
3158.88	1.21	0.14	0.09	0.92	0.00	19.84	39.07	41.10	0.33	0.19	0.14	0.29	0.22	0.38	
3161.75	1.49	0.17	0.08	0.91	0.00	20.47	41.89	37.65	0.32	0.20	0.14	0.28		0.44	※
3162.62	1.50	0.15	0.09	0.64	0.03	22.21	26.87	50.92	0.35	0.19	0.07	0.29		0.38	※
3165.87	1.47	0.23	0.13	0.97	0.00	21.55	45.18	33.27	0.33	0.17	0.12	0.16	0.50	0.35	
3169.19	1.17	0.48	0.36	0.58	0.00	17.11	40.80	42.09	0.36	0.19	0.21	0.13	0.49	0.38	
3171.29	1.06	0.26	0.17	0.71	0.03	19.26	39.09	41.65	0.32	0.17	0.16	0.28	0.40	0.40	
3174.75	1.26	0.36	0.23	0.68	0.00	14.21	45.06	40.73	0.36	0.19	0.16	0.15	0.54	0.41	
3177.20	1.28	0.44	0.32	0.56	0.06	22.34	33.62	44.04	0.37	0.23	0.21	0.12	0.44	0.30	
3177.55	1.07	0.25	0.22	0.49	0.00	22.08	37.87	40.05	0.37	0.21	0.09	0.33	0.34	0.38	※
3183.36	1.40	0.30	0.17	0.65	0.00	19.00	37.49	43.51	0.31	0.18	0.15	0.24	0.52	0.41	※
3186.56	1.32	1.01	0.71	0.72	0.18	28.54	30.06	41.40	0.34	0.21	0.20	0.20	0.51	0.40	
3190.57	1.13	1.34	1.42	0.88	0.87	12.54	34.55	52.91	0.45	0.32	0.18	0.07	0.76	0.41	※
3196.30	1.50	0.95	0.59	1.64	0.18	20.70	37.28	42.02	0.32	0.19	0.15	0.22	0.46	0.42	
3200.73	1.42	1.58	1.26	0.86	0.66	17.88	34.41	47.72	0.40	0.24	0.19	0.11	0.67	0.48	※
3203.21	1.51	1.26	0.99	0.98	0.23	22.09	36.58	41.33	0.35	0.20	0.27	0.13	0.52	0.37	
3208.33	1.42	1.63	1.27	0.66	0.39	18.48	35.83	45.69	0.35	0.19	0.25	0.10	0.52	0.29	
3212.16	0.94	0.92	1.18	0.39	0.00	16.97	36.91	46.12	0.42	0.26	0.13	0.15		0.45	※
3217.51	1.07	1.73	2.32	1.00	0.99	13.10	35.79	51.11	0.42	0.25	0.19	0.06	0.74	0.45	
3217.98	1.02	1.35	1.85	0.82	1.55	12.52	38.23	49.26	0.40	0.23	0.22	0.06	0.67	0.47	
3223.23	1.16	1.64	1.91	0.84	1.00	14.28	35.65	50.07	0.39	0.22	0.20	0.05	0.79	0.42	
3227.14	1.13	1.55	1.86	0.83	0.94	14.81	37.11	48.09	0.38	0.21	0.19	0.04	0.74	0.48	※
3237.77	1.16	1.32	1.67	1.79	0.00	14.35	36.35	49.30	0.40	0.21	0.20	0.05	0.61	0.44	
3249.31	0.74	1.99	3.37	0.88	0.50	17.54	34.22	48.24	0.37	0.21	0.24	0.05	0.74	0.42	
3263.19	1.06	1.75	2.40	1.08	1.12	12.01	34.64	53.35	0.43	0.27	0.19	0.05	0.78	0.44	※
3267.19	1.15	1.75	2.12	1.15	1.01	11.65	34.13	54.22	0.44	0.28	0.21	0.04	0.80	0.45	
3274.00	1.05	1.77	2.35	0.95	1.36	11.84	33.47	54.69	0.44	0.28	0.19	0.05	0.80	0.48	※
3276.99	1.10	1.75	2.26	1.07	1.27	11.48	33.95	54.57	0.44	0.29	0.20	0.05	0.81	0.45	※

(*continued on next page*)

Appendix Table 3 (*continued*)

Depth, m	Pr/Ph	Pr/nC_{17}	Ph/nC_{18}	21−/22+	β/C_{max}	27%	28%	29%	20S, %	ββ, %	G/H	Ts/Tm	ETR	C_{35}/C_{34}	Remark
3279.11	0.99	1.78	2.55	0.93	2.00	11.35	33.60	55.04	0.41	0.24	0.19	0.04	0.83	0.48	※
3284.63	1.02	1.74	2.53	1.09	1.92	11.41	32.34	56.26	0.38	0.22	0.24	0.04	0.83	0.44	
3286.70	1.01	1.49	2.17	1.44	1.09	14.47	31.90	53.63	0.43	0.25	0.20	0.05			※
3294.48	1.00	2.25	3.05	0.68	0.21	6.32	32.54	61.15	0.38	0.31	0.17	0.58		0.28	
3296.61	1.04	1.96	3.08	1.26	2.82	11.80	34.78	53.43	0.40	0.23	0.13	0.12	0.64	0.43	
3301.19	0.98	1.59	2.58	1.26	1.24	12.99	36.04	50.97	0.41	0.23	0.11	0.13	0.71	0.46	
3302.68	0.94	0.92	1.00	0.39	0.11	10.66	51.99	37.35	0.43	0.25	0.13	0.15	0.45	0.47	
3306.47	0.85	1.51	2.62	1.14	1.67	14.74	33.93	51.33	0.40	0.23	0.15	0.12	0.70	0.41	※
3308.42	0.88	1.48	2.22	0.56	1.00	12.70	40.58	46.72	0.41	0.24	0.14	0.12	0.67	0.46	※
3311.18	1.03	1.69	2.36	1.06	2.64	17.47	36.78	45.74	0.43	0.25	0.16	0.17	0.58	0.36	※
3313.65	0.99	1.88	2.50	0.74	1.47	8.71	30.37	60.93	0.39	0.34	0.21	0.60	0.30	0.35	
3319.96	1.01	1.24	1.74	1.80	0.85	18.38	33.04	48.58	0.42	0.26	0.19	0.28	0.51	0.41	※
3323.38	0.95	1.38	1.73	0.88	1.82	18.18	33.71	48.11	0.42	0.29	0.20	0.35	0.47	0.44	※
3327.94	1.45	0.86	0.62	1.02	0.73	20.06	35.88	44.07	0.44	0.28	0.21	0.27	0.46	0.44	
3336.38	1.17	0.39	0.30	0.53	0.07	20.30	37.58	42.12	0.43	0.31	0.12	0.44	0.42	0.44	

Note: Pr/Ph = Pristane/Phytane; Pr/C_{17} = Pristane/C_{17} n-alkane; Ph/C_{18} = Phytane/C_{18} n-alkane; 21−/22+ = $\sum C_{<21}$ n-alkane/$\sum C_{>22}$ n-alkane; β/C_{max} = β-carotane/main carbon peak; 27% = C_{27} steranes/(C_{27} steranes + C_{28} steranes + C_{29} steranes); 28% = C_{28} steranes/(C_{27} steranes + C_{28} steranes + C_{29} steranes); 29% = C_{29} steranes/(C_{27} steranes + C_{28} steranes + C_{29} steranes); C_{27}/(C_{27}+C_{29}) = C_{27} steranes/(C_{27} steranes + C_{29} steranes); 20S(%) = C_{29} sterane ααα20S/(20S + 20R); ββ(%) = C_{29} sterane αββ/(αββ+ααα); G/H = Gammacerane/C_{30} hopane; Ts/Tm = 18α(H)-22,29,30- trisnorneohopane/17α(H)-22,29,30-trisnorhopane; ETR = (C_{28} + C_{29})/(C_{28} + C_{29} + Ts); C_{35}/C_{34} = C_{35} 22S/C_{34} 22S hopane. The datas remarked with ※ is from Ding X.J. et al. (2019).

References

Anderson, T.F., Arthur, M.A., 1983. Stable isotopes of oxygen and carbon and their application to sedimentology and palaeoenvironmental problems. In: Arthur, M.A., Anderson, T.F. (Eds.), Stable Isotopes in Sedimentary, 155. SEPM Society for sedimentary geology. https://doi.org/10.2110/scn.83.01.0000.

Albrecht, P., Vandenbroucke, M., Mandengue, M., 1976. Geochemical studies on the organic matter from the Douala Basin (Cameroon)-I. Evolution of the extractable organic matter and the formation of petroleum. Geochem. Cosmochim. Acta 40, 791–799. https://doi.org/10.1016/0016-7037(76)90031-4.

Arthur, M.A., Dean, W.E., 1998. Organic matter production and preservation and evolution of anoxia in the Holocene Black Sea. Paleoceanography 13, 395–411. https://doi.org/10.1029/98PA01161.

Berner, R.A., 1984. Sedimentary pyrite formation: an update. Geochem. Cosmochim. Acta 48 (4), 605–615. https://doi.org/10.1016/0016-7037(84)90089-9.

Berner, R.A., Raiswell, R., 1983. Burial of organic carbon and pyrite sulfur in sediments over phanerozoic time: a new theory. Geochem. Cosmochim. Acta 47 (5), 855–862. https://doi.org/10.1016/0016-7037(83)90151-5.

Bohacs, K.M., Carroll, A.R., Neal, J.E., et al., 2000. Lake-basin type, source potential, and hydrocarbon character: An integrated sequence-stratigraphic geochemical framework. In: Gierlowski-Kordesch, E.H., Kelts, K.R. (Eds.), Lake Basins through Space and Time. American Association of Petroleum Geologists Studies in Geology, pp. 3–34.

Bradley, W.H., 1970. Green River oil shale-concept of origin extended: an interdisciplinary problem being attacked from both ends. Bull. Geol. Soc. Am. 81, 985–1000. https://doi.org/10.1130/0016-7606(1970)81[985:GROSOO]2.0.CO;2.

Cao, Z., Jiang, H., Zeng, J.H., 2021. Nanoscale liquid hydrocarbon adsorption on clay minerals: a molecular dynamics simulation of shale oils. Chem. Eng. J. 420, 127578. https://doi.org/10.1016/j.cej.2020.127578.

Cao, Z., Liu, G.D., Kong, Y.H., et al., 2016. Lacustrine tight oil accumulation characteristics: Permian Lucaogou Formation in Jimusaer Sag, Junggar Basin. Int. J. Coal Geol. 153, 37–51. https://doi.org/10.1016/j.coal.2015.11.004.

Cao, Z., Liu, G.D., Xiang, B.L., 2015. Geochemical characteristics of crude oil from a tight oil reservoir in the Lucaogou Formation, Jimusar Sag, Junggar Basin. AAPG (Am. Assoc. Pet. Geol.) Bull. 101, 39–72. https://doi.org/10.1306/05241614182.

Cao, J., Yang, R.F., Yin, W., et al., 2018. Mechanism of organic matter accumulation in residual bay environments: the Early Cretaceous Qiangtang Basin, Tibet. Energy & Fuels 32 (2), 1024–1037. https://doi.org/10.1021/acs.energyfuels.7b02248.

Carroll, A.R., Bohacs, K.M., 2001. Lake type controls on petroleum source rock potential in nonmarine basins. AAPG (Am. Assoc. Pet. Geol.) Bull. 85, 1033–1053. https://doi.org/10.1306/64EDA6EA-1724-11D7-8645000102C1865D.

Chen, Z.H., Cao, Y.C., Wang, X.L., et al., 2016. Oil origin and accumulation in the Paleozoic Chepaizi–Xinguang field, Junggar Basin, China. J. Asian Earth Sci. 115, 1–15. https://doi.org/10.1016/j.jseaes.2015.09.019.

Connan, J., 1973. Diagenese naturelle et diagenese artificielle de la matiere organique a element vegetaux predominant. In: Tissot, B.P., Bienner, F. (Eds.), Advances in Organic Geochemistry. Editions Technip, Paris, pp. 73–95.

Cranwell, P.A., Eglinton, G., Robinson, N., 1987. Lipids of aquatic organisms as potential contributors to lacustrine sediments-II. Org. Geochem. 11, 513–527. https://doi.org/10.1016/0146-6380(87)90007-6.

Damsté, J.S.S., Kenig, F., Koopmans, M.P., et al., 1995. Evidence for gammacerane as an indicator of water column stratification. Geochem. Cosmochim. Acta 59, 1895–1900.

Davison, W., 1988. In: Fleet, A.J., Kelts, K., Talbot, M.R. (Eds.), Interactions of Iron, Carbon and Sulphur in Marine and Lacustrine Sediments, 1988, Lacustrine Petroleum Source Rocks, 40. Geological Society Special Publication No., pp. 131–138

Demaison, G.J., Moore, G.T., 1980. Anoxic environments and oil source bed genesis. Org. Geochem. 2, 9–31. https://doi.org/10.1016/0146-6380(80)90017-0.

Didyk, B.M., Simoneit, B.R.T., Brassell, S.C., et al., 1978. Organic geochemical indicators of palaeoenvironmental conditions of sedimentation. Nature 272, 216–222. https://doi.org/10.1038/272216a0.

Ding, X.J., Liu, G.D., Zha, M., et al., 2015. Characteristics and origin of lacustrine source rocks in the lower Cretaceous, Erlian Basin, Northern China. Mar. Petrol. Geol. 66, 939–955. https://doi.org/10.1016/j.marpetgeo.2015.08.002.

Ding, X.J., Liu, G.D., Zha, M., et al., 2016. Geochemical characterization and depositional environment of source rocks of small fault basin in Erlian Basin, northern China. Mar. Petrol. Geol. 69, 231–240. https://doi.org/10.1016/j.marpetgeo.2015.11.006.

Ding, X.J., Gao, C.H., Zha, M., et al., 2017. Depositional environment and factors controlling β-carotane accumulation: a case study from the Jimsar Sag, Junggar Basin, northwestern China. Palaeogeogr. Palaeoclimatol. Palaeoecol. 485, 833–842. https://doi.org/10.1016/j.palaeo.2017.07.040.

Ding, X.J., Qu, J.X., Imin, A., et al., 2019. Organic matter origin and accumulation in tuffaceous shale of the lower Permian Lucaogou Formation, Jimsar Sag. J. Petrol. Sci. Eng. 179, 696–706. https://doi.org/10.1016/j.petrol.2019.05.004.

Ding, W.J., Hou, D.J., Jiang, L., et al., 2019. High abundance of carotanes in the brackish-saline lacustrine sediments: a possible cyanobacteria source? Int. J. Coal Geol. 219, 103373. https://doi.org/10.1016/j.coal.2019.103373.

Duggen, S., Croot, P., Schacht, U., et al., 2007. Subduction zone volcanic ash can fertilize the surface ocean and stimulate phytoplankton growth: evidence from biogeochemical experiments and satellite data. Geophys. Res. Lett. 34, 95–119. https://doi.org/10.1029/2006GL027522.

Eglinton, G., Hamilton, R.J., 1967. Leaf epicuticular waxes: the waxy outer surfaces of most plants display a wide diversity of fine structure and chemical constituents. Science 156, 1322–1335. https://doi.org/10.1126/science.156.3780.132.

Eugster, H.P., Surdam, R.C., 1973. Depositional environment of the Green River formation: a preliminary report. Bull. Geol. Soc. Am. 86, 319–334. https://doi.org/10.1130/0016-7606(1973)842.0.CO;2.

Fike, D.A., Grotzinger, J.P., Pratt, L.M., et al., 2006. Oxidation of the Ediacaran Ocean. Nature 444, 744–747. https://doi.org/10.1038/nature05345.

Fischer, G., Wefer, G., 1999. Use of Proxies in Paleoceanography: Examples from the South Atlantic. Springer-Verlag Berlin Heidelberg GmbH, pp. 428–430.

Glumac, B., Spivak-Birndorf, M.L., 2002. Stable isotope of carbon as an invaluable stratigraphic tool: an example from the Cambrian of the northern Appalachians, USA. Geology 30, 563–566. https://doi.org/10.1130/0091-7613(2002)030<0563:SIOCAA>2.0.CO;2.

Hall, P.B., Douglas, A.G., 1983. The distribution of cyclic alkanes in two lacustrine deposits. In: Bjorøy, M., et al. (Eds.), In Advances in Organic Geochemistry, pp. 576–587.

Hao, F., Zhou, X.H., Zhu, Y.M., et al., 2009. Mechanisms for oil depletion and enrichment on the Shijiutuo uplift, Bohai Bay basin, China. AAPG (Am. Assoc. Pet. Geol.) Bull. 93, 1015–1037. https://doi.org/10.1306/04140908156.

Hao, F., Zhou, X.H., Zhu, Y.M., et al., 2011. Lacustrine source rock deposition in response to coevolution of environments and organisms controlled by tectonic subsidence and climate, Bohai Bay basin, China. Org. Geochem. 42, 323–339. https://doi.org/10.1016/j.orggeochem.2011.01.010.

He, Z.T., Yin, X.D., Jiang, S., et al., 2022. Source rock classification, maturity and their implications in paleoenvironment reconstruction in the Zhu III sub-basin, China. J. Petrol. Sci. Eng. 216, 110799. https://doi.org/10.1016/j.petrol.2022.110799.

Hedges, J.I., Keil, R.G., 1995. Sedimentary organic matter preservation: an assessment and speculative synthesis. Mar. Chem. 49, 81–115. https://doi.org/10.1016/

0304-4203(95)00008-F.
Hillier, S., 2003. Quantitative analysis of clay and other minerals in sandstones by X-ray powder diffraction (XRPD). In: Worden, R., Morad, S. (Eds.), Clay Mineral Cements in Sandstones. International Association of Sedimentologist, Special Publication, Oxford, International, pp. 213–251. https://doi.org/10.1002/9781444304336.ch11.
Hoefs, J., 2009. Stable Isotope Geochemistry, sixth ed. Springer-Verlag Berlin Heidelberg, pp. 159–160.
Hoffman, P.E., Kaufman, A.J., Halverson, G.P., et al., 1998. A neoproterozoic snowball earth. Science 281, 1342–1346. https://doi.org/10.1126/science.281.5381.1342.
Hou, M.G., Zha, M., Ding, X.J., et al., 2021. Source and accumulation process of Jurassic biodegraded oil in the Eastern Junggar Basin, NW China. Petrol. Sci. 18 (4), 1033–1046. https://doi.org/10.1016/j.petsci.2021.07.010.
Hu, T., Pang, X.Q., Jiang, F.J., et al., 2021. Movable oil content evaluation of lacustrine organic-rich shales: methods and a novel quantitative evaluation model. Earth Sci. Rev. 214, 103545. https://doi.org/10.1016/j.earscirev.2021.103545.
Hu, T., Pang, X.Q., Wang, X.L., et al., 2017. Source rock characteristics of Permian Lucaogou Formation in the Jimusar Sag, Junggar Basin, northwest China, and its significance on tight oil source and occurrence. Geol. J. 52, 624–645. https://doi.org/10.1002/gj.2818.
Hu, T., Pang, X.Q., Xu, T.W., et al., 2022. Identifying the key source rocks in heterogeneous saline lacustrine shales: Paleogene shales in the Dongpu Depression, Bohai Bay Basin, eastern China. AAPG (Am. Assoc. Pet. Geol.) Bull. 106 (6), 1325–1356. https://doi.org/10.1306/01202218109.
Huang, D.F., Li, J.C., Zhou, Z.H., et al., 1984. Evolution and Hydrocarbon Generation Mechanism of Terrestrial Organic Matter. Petroleum industry press, Beijing, pp. 25–29 (in Chinese).
Isozaki, Y., Kawahata, H., Ota, A., 2007. A unique carbon isotope record across the Guadalupian-Lopingian (Middle-Upper Permian) boundary in mid-oceanic paleo-atoll carbonates: the high-productivity "Kamura event" and its collapse in Panthalassa. Global Planet. Change 55, 21–38. https://doi.org/10.1016/j.gloplacha.2006.06.006.
Jarvie, D.M., Hill, R.J., Ruble, T.E., et al., 2007. Unconventional shale-gas systems: the Mississippian Barnett Shale of north-central Texas as one model for thermogenic shale-gas assessment. AAPG (Am. Assoc. Pet. Geol.) Bull. 91, 475–499. https://doi.org/10.1306/12190606068.
Jiang, Y.Q., Liu, Y.Q., Yang, Z., et al., 2015. Characteristics and origin of tuff-type tight oil in Jimusar depression, Junggar Basin, NW China. Petrol. Explor. Dev. 42, 741–749. https://doi.org/10.1016/S1876-3804(15)30077-X.
Jin, Z.J., Zhu, R.K., Liang, X.P., et al., 2021. Several issues worthy of attention in current lacustrine shale oil exploration and development. Petrol. Explor. Dev. 48 (6), 1471–1484. https://doi.org/10.1016/S1876-3804(21)60303-8.
Kaufman, A.J., Knoll, G.M., 1995. Neoproterozoic variations in the C-isotopic composition of seawater: stratigraphic and biogeochemical implications. Precambrian Res. 73, 27–49. https://doi.org/10.1016/0301-9268(94)00070-8.
Jørgensen, B.B., 1982. Mineralization of organic matter in the sea bed—the role of sulphate reduction. Nature 296, 643–645.
Katz, B.J., 1990. Controls on distribution of lacustrine source rocks through time and space. In: Katz, B.J. (Ed.), Lacustrine Basin Exploration: Case Studies and Modern Analogs, 50. AAPG Memoir, pp. 61–76.
Katz, B.J., 2005. Controlling factors on source rock development-a review of productivity, preservation, and sedimentation rate. In: Harris, N.B. (Ed.), The Deposition of Organic Carbon Rich Sediments: Models, Mechanisms, and Consequences. Society of Sedimentary Geology, pp. 7–16.
Katz, B., Lin, F., 2014. Lacusrine basin unconventional resource plays: key differences. Mar. Petrol. Geol. 56, 255–265. https://doi.org/10.1016/j.marpetgeo.2014.02.013.
Kelts, K., 1988. Environments of deposition of lacustrine petroleum source rocks: an introduction. In: Fleet, A.J., Kelts, K., Talbot, M.R. (Eds.), 1988, Lacustrine Petroleum Source Rocks, 40. Geological Society Special Publication, pp. 3–26.
Keym, M., Dieckmann, V., Horsfield, B., et al., 2006. Source rock heterogeneity of the Upper Jurassic Draupne Formation, north Viking Graben, and its relevance to petroleum generation studies. Org. Geochem. 37, 220–243. https://doi.org/10.1016/j.orggeochem.2005.08.023.
Kou, J.Y., 2015. Diagenesis of Tight Reservoir in Continental Rift Basin—A Case Study of Lucaogou Formation of Jimsar Sag in Xinjiang. Northwest University. Master's dissertation (in Chinese).
Kuang, L.C., Tang, Y., Lei, D.W., et al., 2012. Formation conditions and exploration potential of tight oil in the Permian saline lacustrine dolomitic rock, Junggar Basin, NW China. Petrol. Explor. Dev. 39, 700–711. https://doi.org/10.1016/S1876-3804(12)60095-0.
Kuang, L.C., Hou, L.H., Wu, S.T., et al., 2022. Organic matter occurrence and pore-forming mechanisms in lacustrine shales in China. Petrol. Sci. 19 (4), 1460–1472. https://doi.org/10.1016/j.petsci.2022.03.005.
Lallier-Vergès, E., Bertrand, P., Desprairies, A., 1993a. Organic matter composition and sulfate reduction intensity in Oman Margin sediments. Mar. Geol. 112, 57–69. https://doi.org/10.1016/0025-3227(93)90161-N.
Lallier-Vergès, E., Bertrand, P., Huc, A.Y., et al., 1993b. Control of the preservation of organic matter by productivity and sulphate reduction in Kimmeridgian shales from Dorset (UK). Mar. Petrol. Geol. 10, 600–605. https://doi.org/10.1016/0264-8172(93)90062-W.
Langmann, B., Zakšek, K., Hort, M., et al., 2010. Volcanic ash as fertiliser for the surface ocean. Atmos. Chem. Phys. 10, 3891–3899.
Li, P., Liu, Q.Y., Bi, H., et al., 2021. Analysis of the difference in organic matter preservation in typical lacustrine shale under influence of volcanism and transgression. Acta Geol. Sin. 95, 632–642. https://doi.org/10.19762/j.cnki.-dizhixuebao.2021123 (in Chinese).
Li, W.H., Lu, S.F., Tan, Z.Z., et al., 2017. Lacustrine source rock deposition in response to coevolution of the paleoenvironment and formation mechanism of organic-rich shales in the Biyang depression. Nanxiang Basin. Energy & Fuels 31, 13519–13527. https://doi.org/10.1021/acs.energyfuels.7b02880.
Lin, M.R., Xi, K.L., Cao, Y.C., et al., 2021. Petrographic features and diagenetic alteration in the shale strata of the Permian Lucaogou Formation, Jimusar Sag, Junggar Basin. J. Petrol. Sci. Eng. 203, 108684. https://doi.org/10.1016/j.petrol.2021.108684.
Liu, Q.Y., Li, P., Jin, Z.J., et al., 2022. Organic-rich formation and hydrocarbon enrichment of lacustrine shale strata: A case study of Chang 7 Member. Sci. China Earth Sci. 65, 118–138. https://doi.org/10.1007/s11430-021-9819-y.
Liu, B., Lv, Y.F., Zhao, R., et al., 2012. Formation overpressure and shale oil enrichment in the shale system of Lucaogou Formation, Malang Sag, Santanghu Basin, NW China. Petrol. Explor. Dev. 39 (6), 744–750. https://doi.org/10.1016/S1876-3804(12)60099-8.
Liu, Q.Y., Li, P., Jin, Z.J., 2021. Preservation of organic matter in shale linked to bacterial sulfate reduction (BSR) and volcanic activity under marine and lacustrine depositional environments. Mar. Petrol. Geol. 127, 104950. https://doi.org/10.1016/j.marpetgeo.2021.104950.
Luo, Q.Y., Gong, L., Qu, Y.S., et al., 2018. The tight oil potential of the Lucaogou Formation from the southern Junggar Basin, China. Fuel 234, 858–871. https://doi.org/10.1016/j.fuel.2018.07.002.
Marcel, C.H., Vernal, A.D., 2007. Proxies in Late Cenozoic Paleoceanography (Developments in Marine Geology 1). Elsevier, pp. 752–756.
Magaritz, M.M., 1983. Carbon and oxygen isotope composition of recent and ancient coated grains. In: Peryt, T.M. (Ed.), Coated Grains. Springer-Verlag, Berlin, pp. 27–37.
Meyers, P.A., 1997. Organic geochemical proxies of paleoceanographic, paleolimnologic, and paleoclimatic processes. Org. Geochem. 27, 213–250. https://doi.org/10.1016/S0146-6380(97)00049-1.
Mckenzie, J.A., 1982. Carbon-13 cycle in Lake Greifen: a model for restricted ocean sub-basins. In: Schlanger, S.O., Cita, M.B. (Eds.), Nature and Origin of Cretaceous Carbon Rcih Facies. University of California, pp. 197–207.
McKenzie, J.A., 1985. Carbon isotopes and productivity in the lacustrine and marine environment. In: Stumm, W. (Ed.), Chemical Processes in Lakes. Swiss Federal Insitute of Technology, Zurich, pp. 99–118.
Morel, F.M.M., Price, N.M., 2003. The biogeochemical cycles of trace metals in the oceans. Science 300, 944. https://doi.org/10.1126/science.1083545.
Oana, S., Deevey, E.S., 1960. Carbon 13 in lake waters and its possible bearing on paleolimnology. Am. J. Sci. 258, 253–272. https://doi.org/10.2105/AJPH.50.12.1967-b.
Pan, Y.S., Huang, Z.L., Li, T.J., et al., 2020. Environmental response to volcanic activity and its effect on organic matter enrichment in the Permian Lucaogou Formation of the Malang Sag, Santanghu Basin, Northwest China. Palaeogeogr. Palaeoclimatol. Palaeoecol. 560, 110024. https://doi.org/10.1016/j.palaeo.2020.110024.
Pang, X.J., Wang, G.W., Kuang, L.C., et al., 2022. Prediction of multiscale laminae structure and reservoir quality in fine-grained sedimentary rocks: the Permian Lucaogou Formation in Jimusar Sag. Junggar Basin. https://doi.org/10.1016/j.petsci.2022.08.001.
Pedersen, T.F., Calvert, S., 1990. Anoxia vs. productivity: what controls the formation of organic carbon rich sediments and sedimentary rocks? AAPG (Am. Assoc. Pet. Geol.) Bull. 4, 454–466. https://doi.org/10.1306/0C9B232B-1710-11D7-8645000102C1865D.
Peters, K.E., 1986. Guidelines for evaluating petroleum source rock using programmed pyrolysis. AAPG (Am. Assoc. Pet. Geol.) Bull. 70, 318–329. https://doi.org/10.1306/94885688-1704-11D7-8645000102C1865D.
Peters, K.E., Cassa, M.R., 1991. Applied source rock geochemistry: chapter 5: Part II. Essential elements. In: Magoon, L.B., Dow, W.G. (Eds.), The Petroleum System-From Source to Trap. AAPG Memoir, pp. 93–120.
Peters, K.E., Fraser, T.H., Amris, W., et al., 1999. Geochemistry of crude oils from eastern Indonesia. AAPG (Am. Assoc. Pet. Geol.) Bull. 83, 1927–1942. https://doi.org/10.1306/E4FD4643-1732-11D7-8645000102C1865D.
Peters, K.E., Moldowan, J.M., 1991. Effects of source, thermal maturity, and biodegradation on the distribution and isomerization of homohopanes in petroleum. Org. Geochem. 17, 47–61. https://doi.org/10.1016/0146-6380(91)90039-M.
Peters, K.E., Walters, C.C., Moldowan, J.M., 2005. The Biomarker Guide: Biomarkers and Isotopes in Petroleum Exploration and Earth History, second ed., 2. Cambridge University Press, Cambridge.
Philp, R.P., Chen, J.H., Fu, J.M., et al., 1992. A geochemical investigation of crude oils and source rocks from Biyang Basin, China. Org. Geochem. 18, 933–945. https://doi.org/10.1016/0146-6380(92)90060-B.
Qiu, Z., Lu, B., Shi, Z.S., et al., 2016a. Residual accumulation and resource assessment of shale oil from the Permian Lucaogou Formation in Jimusar Sag. Nat. Gas Geosci. 27, 1817–1827. https://doi.org/10.11764/j.issn.1672-1926.2016.10.1817 (in Chinese).
Qiu, Z., Shi, Z.S., Dong, D., et al., 2016b. Geological characteristics of source rock and reservoir of tight oil and its accumulation mechanism: A case study of Permian Lucaogou Formation in Jimusar Sag, Junggar Basin. Petroleum Exploration and Development 43 (6), 1013–1024. https://doi.org/10.1016/S1876-3804(16)30118-5.
Raiswell, R., Berner, R.A., 1985. Pyrite formation in euxinic and semi-euxinic

sediments. Am. J. Sci. 285, 710–724. https://doi.org/10.2475/ajs.285.8.710.
Roberts, A.P., 2015. Magnetic mineral diagenesis. Earth Sci. Rev. 151, 1–47. https://doi.org/10.1016/j.earscirev.2015.09.010.
Reeburgh, W.S., 1980. Anaerobic methane oxidation: rate depth distributions in Skan Bay sediments. Earth Planet Sci. Lett. 47, 345–352. https://doi.org/10.1016/0012-821X(80)90021-7.
Sarnthein, M., Winn, K., 1990. Reconstruction of low and middle latitude export productivity, 30,000 years to Present: implications for global carbon reservoirs. In: Schlesinger, M.E. (Ed.), Climate-Ocean Interaction. Kluwer, Dordrecht, pp. 319–342. https://doi.org/10.1007/978-94-009-2093-4_16.
Seifert, W.K., Moldowan, J.M., 1978. Applications of steranes, terpanes and monoaromatics to the maturation, migration and source of crude oils. Geochem. Cosmochim. Acta 42, 77–95. https://doi.org/10.1016/0016-7037(78)90219-3.
Shao, Y., Yang, Y.Q., Wan, M., et al., 2015. Sedimentary characteristic and facies evolution of Permian Lucaogou Formation in Jimsar Sag, Junggar Basin. Xinjiang. Pet. Geol. 36, 635–641. https://doi.org/10.7657/XJPG20150602 (in Chinese).
Summons, R.E., Hope, J.M., Swart, R., et al., 2008. Origin of Nama Basin bitumen seeps: petroleum derived from a Permian lacustrine source rock traversing southwestern Gondwana. Org. Geochem. 39, 589–607. https://doi.org/10.1016/j.orggeochem.2007.12.002.
Sýkorová, I., Pickel, W., Christanis, K., et al., 2005. Classification of liptinite – ICCP system 1994. Int. J. Coal Geol. 169, 40–61. https://doi.org/10.1016/j.coal.2004.06.006.
Tang, Y., Cao, J., He, W.J., et al., 2021. Discovery of shale oil in alkaline lacustrine basins: the late Paleozoic Fengcheng formation, Mahu Sag, Junggar Basin, China. Petrol. Sci. 18 (5), 1281–1293. https://doi.org/10.1016/j.petsci.2021.04.001.
Turgeon, S.C., Creaser, R.A., 2008. Cretaceous oceanic anoxic event 2 triggered by a massive magmatic episode. Nature 454, 323–327. https://doi.org/10.1038/nature07076.
Volkman, J.K., 1983. A review of sterol markers for marine and terrigenous organic-matter. Org. Geochem. 9, 83–99. https://doi.org/10.1016/0146-6380(86)90089-6.
Volkman, J.K., Barrett, S.M., Blackburn, S.I., et al., 1998. Microalgal biomarkers: a review of recent research developments. Org. Geochem. 29, 1163–1179. https://doi.org/10.1016/S0146-6380(98)00062-X.
Wang, J., Zhou, L., Liu, J., et al., 2020. Acid-base alternation diagenesis and its influence on shale reservoirs in the Permian Lucaogou Formation, Jimusar Sag, Junggar Basin, NW China. Petrol. Explor. Dev. 47 (5), 962–976. https://doi.org/10.1016/S1876-3804(20)60109-4.
Wang, X.Q., Sun, L., Zhu, R.K., et al., 2015. Application of charging effects in evaluating storage space of tight reservoirs: a case study from Permian Lucaogou Formation in Jimusar sag, Junggar Basin, NW China. Petrol. Explor. Dev. 42, 516–524. https://doi.org/10.1016/S1876-3804(15)30044-6.
Wu, H.G., Hu, W.X., Tang, Y., et al., 2017. The impact of organic fluids on the carbon isotopic compositions of carbonate-rich reservoirs: case study of the Lucaogou Formation in the Jimusaer Sag, Junggar Basin, NW China. Mar. Petrol. Geol. 85, 136–150. https://doi.org/10.1016/j.marpetgeo.2017.05.003.
Xi, K.L., Cao, Y.C., Zhu, R.K., et al., 2015. Rock types and characteristics of tight oil reservoir in Permian Lucaogou Formation, Jimsar Sag. Acta Pet. Sin. 36, 1495–1508. https://doi.org/10.7623/syxb201512004 (in Chinese).
Xie, X.M., Borjigin, T., Zhang, Q., et al., 2015. Intact microbial fossils in the Permian Lucaogou Formation oil shale, Junggar Basin, NW China. Int. J. Coal Geol. 146, 166–178. https://doi.org/10.1016/j.coal.2015.05.011.
Yang, Y.Q., Qiu, L.W., Cao, Y.C., et al., 2017. Reservoir quality and diagenesis of the Permian Lucaogou Formation tight carbonates in Jimsar Sag, Junggar Basin, west China. J. Earth Sci. 28, 1032–1046. https://doi.org/10.1007/s12583-016-0931-6.
Yang, Y.Q., Qiu, L.W., Wan, M., et al., 2019. Depositional model for a salinized lacustrine basin: the Permian Lucaogou Formation, Jimsar Sag, Junggar Basin, NW China. J. Asian Earth Sci. 178, 81–95. https://doi.org/10.1016/j.jseaes.2018.08.021.
Yang, Y.X., Zhang, J.F., Zhang, J.H., et al., 2022. Sedimentary characteristics and main controlling factors of the middle-upper Permian and middle-upper triassic around Bogda mountain of Xinjiang, NW China. Petrol. Explor. Dev. 49 (4), 770–784. https://doi.org/10.1016/S1876-3804(22)60309-4.
Zhang, J.Y., Liu, G.D., Cao, Z., et al., 2019. Characteristics and formation mechanism of multi-source mixed sedimentary rocks in a saline lake, a case study of the Permian Lucaogou Formation in the Jimusaer Sag, northwest China. Mar. Petrol. Geol. 102, 704–724. https://doi.org/10.1016/j.marpetgeo.2019.01.016.
Zheng, M., Li, J.Z., Wu, X.Z., et al., 2016. Physical modeling of oil charging in tight reservoirs: a case study of Permian Lucaogou Formation in Jimsar Sag, Junggar Basin, NW China. Petrol. Explor. Dev. 43 (2), 241–250. https://doi.org/10.1016/S1876-3804(16)30027-1.
Zou, C.N., Yang, Z., Zhu, R.K., et al., 2015. Progress in China's unconventional oil & gas exploration and development and theoretical technologies. Acta Geological Sinca 89, 938–971. https://doi.org/10.1111/1755-6724.12491.
Zou, C.N., Zhu, R.K., Chen, Z.Q., et al., 2019. Organic-matter-rich shales of China. Earth-Science review 189, 51–78. https://doi.org/10.1016/j.earscirev.2018.12.002.